

# 1 **EcoDes-DK15: High-resolution ecological descriptors of vegetation** 2 **and terrain derived from Denmark's national airborne laser scanning** 3 **data set**

4 Jakob J. Assmann<sup>1</sup>, Jesper E. Moeslund<sup>2</sup>, Urs A. Treier<sup>1,3</sup>, Signe Normand<sup>1,3</sup>

5 <sup>1</sup>Department of Biology - Ecoinformatics and Biodiversity, Aarhus University, Aarhus, 8000, Denmark

6 <sup>2</sup>Department of Ecoscience - Biodiversity, Aarhus University, Rønde, 8410, Denmark

7 <sup>3</sup>Department of Biology - Center for Sustainable Landscapes Under Global Change, Aarhus University, Aarhus, 8000,  
8 Denmark

9

10 *Correspondence to:* Jakob J. Assmann ([j.assmann@bio.au.dk](mailto:j.assmann@bio.au.dk))

## 11 **Abstract**

12 Biodiversity studies could strongly benefit from three-dimensional data on ecosystem structure derived from contemporary  
13 remote sensing technologies, such as Light Detection and Ranging (LiDAR). Despite the increasing availability of such data  
14 at regional and national scales, the average ecologist has been limited in accessing them due to high requirements on computing  
15 power and remote-sensing knowledge. We processed Denmark's publicly available national Airborne Laser Scanning (ALS)  
16 data set acquired in 2014/15 together with the accompanying elevation model to compute 70 rasterized descriptors of interest  
17 for ecological studies. With a grain size of 10 m, these data products provide a snapshot of high-resolution measures including  
18 vegetation height, structure and density, as well as topographic descriptors including elevation, aspect, slope and wetness  
19 across more than forty thousand square kilometres covering almost all of Denmark's terrestrial surface. The resulting data set  
20 is comparatively small (~94 GB, compressed 16.8 GB) and the raster data can be readily integrated into analytical workflows  
21 in software familiar to many ecologists (GIS software, R, Python). Source code and documentation for the processing workflow  
22 are openly available via a code repository, allowing for transfer to other ALS data sets, as well as modification or re-calculation  
23 of future instances of Denmark's national ALS data set. We hope that our high-resolution ecological vegetation and terrain  
24 descriptors (EcoDes-DK15) will serve as an inspiration for the publication of further such data sets covering other countries  
25 and regions and that our rasterized data set will provide a baseline of the ecosystem structure for current and future studies of  
26 biodiversity, within Denmark and beyond.

## 27 **1 Introduction**

28 Over the last decades, airborne laser scanning (ALS) has become an established data source for providing fine-resolution  
29 measures of terrain and vegetation structure in ecological research (Moeslund et al., 2019; Guo et al., 2017; Zellweger et al.,  
30 2016). Despite its informative potential and the increasing number of openly available ALS data sets with regional and national  
31 extents (Vo et al., 2016), the uptake of these data sets for large-scale ecological research and applications (such as monitoring  
32 and conservation) has remained comparatively low (Bakx et al., 2019). The low uptake is likely a consequence of the  
33 considerable challenges that remain in handling these very large data sets, which require specialist expertise and software, as  
34 well as substantial amounts of data storage and processing power (Meijer et al., 2020; Vo et al., 2016; Pfeifer et al., 2014).  
35 Here, we address this issue for Denmark by providing a compact set of ecologically relevant measures of terrain characteristics  
36 and vegetation structure derived as raster outputs from the country's national ALS data set with a grain size of 10 m x 10 m.

37 The typical output from an ALS survey is a so-called point cloud that describes the physical structure of the surveyed area in  
38 three-dimensional space (Bakx et al., 2019; Vierling et al., 2008). In brief, short laser pulses are sent out from a Light Detection  
39 and Ranging (LiDAR) sensor mounted on an airplane (or drone) and reflected by surfaces such as bare ground, plants or  
40 buildings. The return timing of the reflected signal is measured and - with the help of information on the sensor's orientation  
41 and position - the precise location of the reflecting surface is determined in geographic space (Vierling et al., 2008). If an  
42 object intercepting the light pulse is smaller than the beam's footprint (e.g., a leaf or a branch of a tree) some of the light may  
43 travel on and trigger a reflection from a second surface (e.g., understory vegetation or the forest floor). A single light pulse  
44 might therefore generate two or even more returns, allowing - to some degree - for the penetration of forest canopies  
45 (Ackermann, 1999). Often, the raw signal is processed by the survey provider and the resulting data is delivered to the end  
46 user in the form of a point cloud of discrete returns, where each point is associated with information on geographic location,  
47 return strength (amplitude), return number, acquisition timing etc. (Vo et al., 2016). For ALS data sets with large extents -  
48 such as Denmark's nationwide data set "DHM/Punktsky" - outputs from many survey flights are co-registered and merged,  
49 resulting in very large point clouds with hundreds of billions of points and data volumes of multiple Terabytes  
50 (Geodatastyrelsen, 2015). For further information on ALS data acquisition, we recommend Vo et al. (2016), Vierling et al.  
51 (2008) and Wagner et al. (2006).

52 Based on point position and neighbourhood context it is possible to separate ground and vegetation returns in ALS point  
53 clouds, allowing for the calculation of descriptors of terrain and vegetation structure. Filtering bare ground from the point  
54 cloud may be achieved with algorithms (Moudrý et al., 2020; Sithole and Vosselman, 2004), while more complex segmentation  
55 of the point clouds into object classes (such as vegetation, buildings, etc.) is done manually or with the help of supervised  
56 machine learning (see Lin et al., 2020 for a recent overview). Early applications for ALS were focussed on generating simple  
57 digital elevation models (DEMs), city and landscape planning, as well as forestry (Ackermann, 1999), but over the last decades  
58 applications have expanded into other fields, including amongst others the calculation of terrain and vegetation measures for

59 ecological research. Terrain derived measures of ecological interest include topographic slope, aspect (i.e., slope direction),  
60 solar irradiation, wetness etc. (e.g., Moeslund et al., 2019; Zellweger et al., 2016; Ceballos et al., 2015), and vegetation  
61 structural descriptors include vegetation density, canopy height diversity, canopy roughness and many more (e.g., Bakx et al.,  
62 2019; Moeslund et al., 2019; Coops et al., 2016). It is important to note that point cloud characteristics may limit the type of  
63 measures that can be meaningfully derived from ALS data (Bakx et al., 2019). This applies especially to the point cloud  
64 density, which needs to be high enough to meaningfully resolve the structure of understory layers in forests (Bakx et al., 2019)  
65 or ecosystems with vegetation of low stature such as grasslands or tundra (Boelman et al., 2016). Nonetheless, even simpler  
66 ALS derived descriptors of terrain and vegetation structure can be of high value for ecological applications, as fieldwork-  
67 derived alternatives are often too costly and difficult to collect over large extents (Vierling et al., 2008).

68 ALS data has provided critical information for research on biodiversity and habitat characteristics over the recent years, and  
69 its importance in ecological research is likely to increase in the future. Numerous biodiversity studies have successfully  
70 deployed ALS to study organisms like plants (Mao et al., 2018; Lopatin et al., 2016; Zellweger et al., 2016; Ceballos et al.,  
71 2015; Moeslund et al., 2013; Leutner et al., 2012), fungi (Peura et al., 2016; Thers et al., 2017), bryophytes, lichens (Moeslund  
72 et al., 2019), mammals (Tweedy et al., 2019; Froidevaux et al., 2016) and birds (see Bakx et al. (2019) for a comprehensive  
73 review) both in open landscapes and in forests. These studies have all emphasized the value of ALS for representing fine-scale  
74 (~ 10 m resolution) terrain or vegetation structural variation important to local biodiversity patterns. Furthermore, Valbuena  
75 et al. (2020) recently considered ALS data to be one of the key resources for deriving ecosystem morphological traits in the  
76 global assessment of Essential Biodiversity Variables (EBVs). Finding ways of making regional and nationwide ALS data  
77 more accessible to the average ecologist is therefore not only a critical priority for accelerating research on regional biodiversity  
78 patterns and species - habitat relationships, but also for the facilitation of global assessments such as those carried out by  
79 IPBES (2019) and alike.

80 To open up opportunities for researchers and practitioners not familiar with ALS processing or without access to the required  
81 facilities, we present a new national ALS based data set for Denmark primarily aimed at ecological research with possible uses  
82 in other disciplines. With a grain size of 10 m, these ecological descriptor (EcoDes) rasters provide a snapshot of high-  
83 resolution measures of vegetation height, structure and density, as well as topographic descriptors including elevation, aspect,  
84 slope and wetness for almost all of Denmark's terrestrial surface between spring 2014 and summer 2015 (DK15). In this  
85 publication, we a) describe the source data and outline the processing workflow (Sect. 2.1-2.3), b) summarise the data set's  
86 main characteristics (Sect. 3.1-3.2), c) describe each descriptor in detail and highlight its use and limitations (Sect. 3.3-3.4), d)  
87 provide guidance on data access and illustrate how the data could be used in an example of ecological landscape classification  
88 (Sect. 4). We finish by e) briefly discussing the general limitations of the data set and processing workflow, as well as providing  
89 perspectives on how the presented data can be complemented with other data sources (Sect. 5). We hope that ease of access

90 and thorough documentation of the EcoDes-DK15 data set will encourage uptake and facilitate the development of future  
91 versions of similar data sets in Denmark and beyond.

## 92 **2 Source data and processing workflow overview**

### 93 **2.1 Denmark - geography and ecology**

94 Located in Northern Europe, Denmark (without Greenland and the Faroe Islands) has an approximate land area of 43 thousand  
95 square kilometres, comprising the large peninsula of Jutland and 443 named islands. The relatively flat (highest point is 171  
96 m above sea level) landscape predominantly consists of arable land and production forest with relatively small patches of  
97 natural or semi-natural areas such as heathlands, grasslands, fresh and salt meadows, bogs, dunes, lakes, streams and deciduous  
98 forests.

### 99 **2.2 ALS and elevation source data**

100 The Danish elevation model (DHM) is an openly available nationwide data set providing various products based on ALS data.  
101 Here, we used the DHM/Point-cloud (DHM/Punktsky), the classified georeferenced ALS point cloud product, and the  
102 DHM/Terrain (DHM/Terræn), the digital elevation model product derived from the point cloud. The DHM data set is currently  
103 maintained by the Agency for Data Supply and Efficiency, Denmark (<https://sdfe.dk/>) and, at the time of writing, can be  
104 downloaded from <https://kortforsyningen.dk/> (continuously updated with new survey data) and <https://datafrodeler.dk>  
105 (versioned). While almost all of Denmark's terrestrial surface was covered by ALS surveys in 2014/15, currently none of the  
106 products provided by the agency contains data exclusively from these surveys. We therefore merged three different versions  
107 of the source data to obtain a dataset that reflects the state of the vegetation in 2014/15 as best as possible, by only containing  
108 vegetation data from 2014/15 and limited amounts from 2013 (Table 1, Sect. 3.6.3; see GitHub code repository for a detailed  
109 description of the merger and more information on the source data sets). The DHM/Point-cloud product is a collection of 1 x  
110 1 km tiles of three-dimensional point clouds with attributes such as position, intensity, point source ID, or classification. Point  
111 classification follows the ASPRS LAS 1.3 standard (ASPRS, 2011), including for example ground, vegetation, and buildings.  
112 The point density is on average 4-5 points per square meter with a horizontal and vertical accuracy of 0.15 and 0.05 metres,  
113 respectively. Additional information on the data sets can be found in Geodatastyrelsen (Geodatastyrelsen, 2015 - in Danish),  
114 Thers et al. (2017), Nord-Larsen et al (2017) and in the quality assessment report by Flatman et al. (2016). The DHM/Point-  
115 cloud product is provided in LAZ-format and in the compound coordinate system for Denmark (ETRS89 / UTM zone 32N +  
116 DVR90 height - EPSG:7416). The DHM/Terrain product is a rasterized digital model of the terrain height above sea level in  
117 0.4 m resolution. This product is provided in a 32-bit GeoTiff format, using the same 1 km x 1 km titling convention and  
118 spatial reference system as the DHM/Point-cloud.

119

120 **Table 1:** Overview of the data sources used for generating the EcoDes-DK15 data set. Three versions of the DHM/Pointcloud  
 121 were merged to obtain a point cloud data set that contained no vegetation points scanned after 2015 and as little vegetation  
 122 points before 2014 as possible. DHM/Terrain tiles were matched sources from the same data source as the corresponding point  
 123 cloud tiles. A copy of the source data is archived on the internal long-term data storage at Aarhus University and is available  
 124 on request. For further information see documentation on GitHub code repository and Sect. 3.6.3.

Data source	Years	Used for	Data provider	Downloaded available from (download date)	Number of tiles
DHM/Pointcloud (DHM/Punktsky)	2007-2018	Vegetation Descriptors	Danish Agency for Data Supply and Efficiency	<a href="https://kortforsyningen.dk/">https://kortforsyningen.dk/</a> (24 April 2020)	38671
DHM/Pointcloud (DHM2015_punktsky)	2007-2018	Vegetation Descriptors	Danish Agency for Data Supply and Efficiency	<a href="https://datafordeler.dk">https://datafordeler.dk</a> (13 September 2020)	10955
DHM/Pointcloud (GST_2014)	2007-2015	Vegetation Descriptors	Danish Agency for Data Supply and Efficiency	<a href="https://kortforsyningen.dk/">https://kortforsyningen.dk/</a> (unknown, before 2017)	47
DHM/Terrain (DHM/Terræn)	2007-2018	Terrain Descriptors	Danish Agency for Data Supply and Efficiency	<a href="https://kortforsyningen.dk/">https://kortforsyningen.dk/</a> (24 April 2020)	38671
DHM/Terrain (DHM2015_terraen)	2007-2018	Terrain Descriptors	Danish Agency for Data Supply and Efficiency	<a href="https://datafordeler.dk">https://datafordeler.dk</a> (13 September 2020)	10955
DHM/Terrain (GST_2014)	2007-2015	Terrain Descriptors	Danish Agency for Data Supply and Efficiency	<a href="https://kortforsyningen.dk/">https://kortforsyningen.dk/</a> (unknown, before 2017)	47

125  
 126 The 1 km x 1 km tiling of the DHM/Terrain 2014/2015 and DHM/Point-cloud data sets 2014/2015 match in extent and  
 127 geolocation. However, a small number of tiles ( $n = 30$ ) in the DHM/Point-cloud data sets did not have corresponding tiles in  
 128 the DHM/Terrain data sets, these were removed prior processing resulting in the total of 49673 tiles shown in Table 1.

### 129 2.3 Processing

130 We processed the source data using OPALS 2.3.2.0 (Pfeifer et al., 2014), Python 2.7 (Van Rossum and Drake Jr, 1995), pandas  
 131 0.24.2 (Reback et al., 2019), SAGA GIS 2.3.2 (Conrad et al., 2015) from OSGeo4W64 and GDAL 2.2.4 (GDAL/OGR  
 132 contributors, 2018) also from OSGeo4W64. Some re-processing was required during the peer review process, for which we  
 133 used GDAL 3.3.3 from OSGeo4W64 (GDAL/OGR contributors, 2021). The large number of tiles and descriptors to be  
 134 calculated, required us to develop a robust processing pipeline, which we realised as a set of Python modules. The source code  
 135 is openly available via a GitHub code repository (see Sect. 6). Processing was carried out on a Dell PowerEdge R740xd

136 computational server (Windows 2012 R2 64-bit Operating System, 2x Intel Xeon Platinum 8180 Processors and 1.536TB  
137 RAM). The processing of the whole data set took approximately 45 days to complete.

138

### 139 2.3.1 Processing workflow

140 To facilitate the processing of the large data set, we first generated a set of compact Python modules providing a programming  
141 interface that allows for the calculation of the individual descriptors outlined in Sect. 3. The individual routines were then  
142 integrated into a Python script mediating the processing workflow in parallel, while carrying out error handling, logging and  
143 progress tracking. The schematic of the processing workflow and the Python modules is outlined in Fig. 1. Detailed information  
144 is available on the GitHub repository, including instructions on how to set up the processing, documentation on the functions  
145 provided by the Python modules, as well as detailed in-text commentary of the code.

146

147 We generated the processing workflow so that it should be possible to adapt it to other point cloud data sets. However, the  
148 effort required in achieving this will vary depending on various features of the point cloud data set in question (such as tiling  
149 and tile naming conventions, input/output grain sizes etc.). A key pre-requisite is that the point cloud is pre-classified, ideally  
150 following the ASPRS LAS 1.1-1.4 standards (ASPRS, 2019). We have also provided a helper script that can be adapted to  
151 generate a raster DTM from the point cloud should this not be available, see the documentation on the GitHub repository for  
152 the details. Finally, the modular nature of the processing workflow allows for only a subset of the output descriptors to be  
153 calculated and the integration of additional processing routines for any new user-defined descriptors.

154

# Processing Workflow Overview

## Inputs

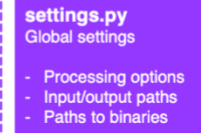
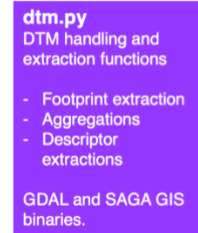
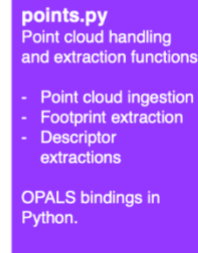
- Nationwide ALS point cloud  
~ 49k tiles
- Nationwide terrain model at 0.4 m res.  
~ 49k tiles



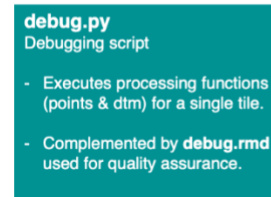
## Outputs

- Ecological variables, raster 10 m res.  
18 x terrain and cover structure descriptors  
~ 49k tiles each

## dk\_lidar Python Modules



## Helper scripts Independent python scripts



155

156 **Figure 1:** Diagram of the processing workflow, the *dk\_lidar* Python module and helper scripts. The workflow requires two  
 157 inputs: a pre-classified set of point cloud tiles and a paired set of digital terrain model (dtm) tiles. The process management is  
 158 handled by the *process\_tiles.py* script which facilitates processing of each tile pair (dtm and point cloud) in parallel and logs  
 159 the progress. For each tile, *process\_tiles.py* calls a specified set of extraction and processing functions from the *dk\_lidar*  
 160 modules. Point cloud extraction functions are specified in *points.py* and terrain model extraction functions are specified in  
 161 *dtm.py*. The *dk\_lidar* modules also contain two further files, *common.py* a script containing specifications of common functions  
 162 used by the *points.py* and *dtm.py*, as well as *settings.py* which is used to set global processing options, specify file paths etc.  
 163 Finally, two helper scripts are provided *progress\_monitor.py* which facilitates progress monitoring and estimates the time  
 164 remaining and *debug.py* a script for testing the workflow for a single tile. Together the Python scripts and modules allow to  
 165 generate the ecological descriptor outputs from the two input data sets. Further documentation of the *dk\_lidar* modules and  
 166 workflow scripts can be found on the GitHub repository associated with this publication:  
 167 <https://github.com/jakobjassmann/ecodes-dk-lidar>.

## 168 3 Data set description and known limitations

### 169 3.1 Extent, projection, resolution and data format

170 EcoDes-DK15 covers the majority of Denmark's land area, including the island of Bornholm (approximate extent: 54.56 °N  
171 to 57.75 °N, 8.07 °E to 15.20 °E). The data is projected in ETRS89 UTM 32 N based on the GRS80 spheroid (EPSG: 25832).  
172 The data set is available as GeoTIFFs with 10 m grain size via a data repository on Zenodo (see Sect. 6). For each descriptor  
173 the nation-wide data are split into 49673 raster tiles of 1 km x 1 km with a 10 m grain size based on 25-fold aggregations of  
174 the 0.4 m national grid of Denmark. A virtual raster mosaic (VRT) file is provided for each descriptor (except the  
175 point\_source\_counts, point\_source\_ids and point\_source\_proportion descriptors), and a file containing the tile footprint  
176 geometries can be used for geographical sub-setting of the data. We also provide masks for inland water and the sea.

177  
178 The final data set consists of just under 94 GB of data (compressed for download 16.8 GB). To reduce the size of the data set  
179 we converted numerical values from floating point precision to 16-bit integers where possible. In some cases, this required us  
180 to stretch the values by a set factor to maintain information content beyond the decimal point. The descriptor conversion factors  
181 are available as a csv file provided with the data set and in Table 2. Missing data is denoted by a value of -9999 throughout  
182 the data set (NODATA-value).

### 183 3.2 Overview and file naming convention

184 An overview of the eighteen terrain and vegetation structure descriptors as well as the auxiliary data provided can be found in  
185 Table 2. Generally, the descriptor names in Table 2 reflect the prefix of the file name of a GeoTiff file within the data set. This  
186 prefix is followed by a suffix representing the unique identifier for each tile based on the UTM coordinates of the tile (see  
187 Sect. 3.4.3 for more detail). When working with the complete data set, tiles from the same descriptor are grouped within a  
188 folder using the same descriptor name as used for the file name prefix. For example, for the tile with the unique id “6239\_446”  
189 the GeoTiff for the “dtm\_10m” descriptor can be found in “dtm\_10m/dtm\_10m\_6239\_446.tif”. The exceptions are the point  
190 counts, vegetation proportions and point source information, please see the relevant sections below for more detail.

191  
192 **Table 2:** Brief overview of the eighteen main EcoDes-DK15 descriptors and descriptor groups, their ecological meaning, unit,  
193 format and conversion factor. See Sect. 3.4 for a detailed description of each descriptor. In addition to the 70 raster layers for  
194 the main descriptors, the data set contains nine layers of auxiliary information (see Sect. 3.7). Note: to obtain the correct unit,  
195 the descriptor value needs to be divided by the conversion factor.

196

Descriptor(s)	Ecological meaning	Unit	Format	Conversion factor	Number of layers
dtm_10m	elevation	m	16-bit integer	100	1



aspect	topographic aspect	degrees	16-bit integer	10	1
slope	topographic slope	degrees	16-bit integer	10	1
heat_load_index	proxy of radiation and wetness	unitless	16-bit integer	10000	1
solar_radiation	solar radiation	MJ x 100 <sup>-1</sup> m <sup>-2</sup> x yr <sup>-1</sup>	32-bit integer	1	1
openness_mean	topographic position	degrees	16-bit integer	1	1
openness_difference	presence of linear landscape features	degrees	16-bit integer	1	1
twi	topographic wetness	unitless	16-bit integer	1000	1
amplitude_mean	complex**	undefined	32-bit float	1	1
amplitude_sd	complex**	undefined	32-bit float	1	1
canopy_height	vegetation height	m	16-bit integer	100	1
normalized_z_mean	average structural height (incl. vegetation and buildings)	m	16-bit integer	100	1
normalized_z_sd	variation in structural height (incl. vegetation and buildings)	m	16-bit integer	100	1
point_counts*	number of returns in ground, water, building and vegetation point classes; total return count and vegetation return counts in height bins	count	16-bit integer	1	30
vegetation_proportion*	proportion of vegetation returns in height bins	proportion	16-bit integer	10000	24
vegetation_density	ratio of vegetation returns to total returns	proportion	16-bit integer	10000	1
canopy_openness	ratio of ground and water returns to total returns	proportion	16-bit integer	10000	1
building_proportion	ratio of building returns to total returns		16-bit integer	10000	1
point_source_info*	point source / flight strip information	varied, see description	varied, see description	varied, see description	4
masks	inland water and sea mask	binary	16-bit integer	1	2
date_stamp*	min, max and mode of GPS dates for all vegetation points	date as YYYYMMDD***	32-bit integer	1	3

197

198

\* Descriptor group containing multiple individual descriptors, see intext description for detail.

199 \*\* The amplitude descriptors are difficult to interpret, but can serve as useful indicators for vegetation classification and  
200 biodiversity studies. Please see intext description for more detail.

201 \*\*\* YYYY = year in four digits, MM = month in two digits, DD = day in two digits.

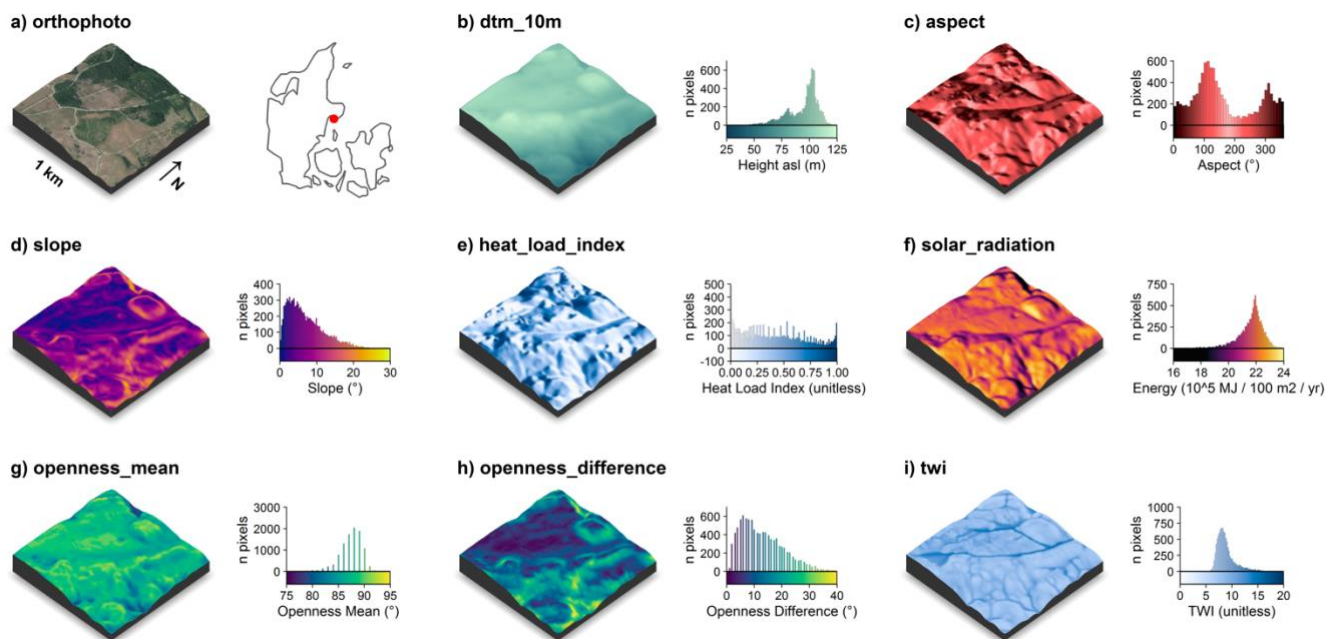
### 202 3.3 Completeness of the data set

203 The processing of the data set was almost completely successful. Processing failed on average for only 18 out of the 49673  
204 tiles per descriptor with a maximum of 65 tiles failing for the *canoy\_height*, *normalized\_z\_mean* and *normalized\_z\_sd*  
205 descriptors. The majority of these tiles were located on the fringes of the data set, including sand spits, sandbanks etc, we  
206 therefore did not attempt re-processing of those tiles. Instead, we generated nodata-value rasters for all missing descriptor -  
207 tile combinations (i.e. we assigned -9999 to all cells in those tiles). We provide a text file listing the affected “nodata” tiles in  
208 the folder of each descriptor (the file is named empty\_tiles\_XXX.txt, where XXX is the descriptor name).

### 209 3.4 Elevation-model derived descriptors

210 The following descriptors were solely derived from the 0.4 m digital elevation model (DHM/Terrain). Visualisations of these  
211 descriptors for an example tile in the Mols Bjerger area are shown in Fig. 2.

212



213

214 **Figure 2:** Illustration of the terrain model derived descriptors for a 1 km x 1 km tile in the Mols Bjerger area (tile id: 6230\_595).

215 An orthophoto and the tile location relative to Denmark are shown in (a). The terrain model (dtm\_10m) is illustrated in (b).

216 The terrain derived descriptors comprise of: c) the topographic aspect, d) the topographic slope, e) the heat load index following

217 Kuehne et al. f) the estimated incident solar radiation, g) the landscape openness mean, h) the landscape openness difference  
218 in the eight cardinal directions and i) the topographic wetness index (TWI) based on Kopecký et al. (2020). For visualisation  
219 purposes, we amplified the altitude above sea-level by a factor of two in the 3D visualisations and divided the solar radiation  
220 values by  $10^5$ . The 3D raster visualisations were generated using the rayshader v0.19.2 package in R (Morgan-Wall, 2020).  
221 Orthophoto provided by the Danish Agency for Data Supply and Efficiency ([https://sdfc.dk/hent-data/fotos-og-geodanmark-  
222 data/](https://sdfc.dk/hent-data/fotos-og-geodanmark-data/)).

### 223 3.4.1 Elevation (dtm\_10m)

224 We aggregated the 0.4 m DEM by mean to match the 10 m x 10 m national grid of the remainder of the data set. We used  
225 *gdalwarp* to carry out the aggregations. Values represent the elevation above sea level in metres (DVR90, EPSG: 5799)  
226 multiplied by a factor of 100, rounded to the nearest integer and converted to 16-bit integer.

### 227 3.4.2 Aspect (aspect)

228 The topographic aspect describes the orientation of a slope in the terrain and may, amongst other things, be related to plant  
229 growth through light and moisture availability. We calculated the aspect in degrees, with  $0^\circ$  indicating North,  $90^\circ$  East,  $180^\circ$   
230 South and  $270^\circ$  West. Values represent the aspect derived from a 10 m aggregate of the elevation model (aggregated by mean  
231 with 32bit floating point precision). Calculations were carried out using *gdaldem* binaries and the “aspect” option, which by  
232 default uses Horn’s method to calculate the aspect (Horn, 1981). To avoid edge effects, all calculations were done on a mosaic  
233 that included the focal tile and all available directly neighbouring tiles (maximum eight). The mosaic was cropped back to the  
234 extent of the focal tile upon completion of the calculations. We then converted the value for each cell from radian to degrees,  
235 multiplied it by a factor of 10, rounded to the nearest integer and stored the results as a 16-bit integer. Finally, we assigned a  
236 value of  $-10$  ( $-1^\circ$ ) to all cells where the slope was  $0^\circ$  (flat). Limitations in the aspect arise in relation to edge effects that occur  
237 where a neighbourhood mosaic is incomplete for a focal tile (i.e., less than eight neighbouring tiles), such as for tiles along the  
238 coastline or at the edge of the covered extent. For those tiles, no aspect can be derived for the rows or columns at the edge of  
239 the mosaic. The cells in those rows and columns have no neighbouring cells and were assigned the no data value (-9999).  
240 Please also note that we calculated the aspect descriptor from the 10 m aggregate of the DTM/Terrain data set rather than  
241 deriving it from the 0.4 m original resolution rasters and then aggregating it. The latter approach could represent the  
242 aspect/slope at the original resolution better (Grohmann, 2015; Moudrý et al., 2019), but would create inconsistencies within  
243 how the remaining DTM/Terrain descriptors are calculated in this dataset.  
244

### 245 3.4.3 Slope (slope)

246 The topographic slope describes the steepness of the terrain and amongst other things may be related to moisture availability,  
247 exposure and erosion. We derived the topographic slope in degrees with a 10 m grain size from a mean aggregate of the

248 elevation model (32bit floating point precision) using the *gdaldem* binaries with the “slope” option, which by default use  
249 Horn’s method to calculate the slope (Horn, 1981). To avoid edge effects, we carried out the calculations on a mosaic including  
250 the focal tile and all available directly neighbouring tiles (maximum eight). The mosaic was cropped back to the extent of the  
251 focal tile upon completion of the calculations. The value for each cell was converted from radian to degrees, multiplied by a  
252 factor of 10, rounded to the nearest integer and stored as a 16-bit integer. Limitations in the slope arise in relation to edge  
253 effects that occur where a neighbourhood mosaic is incomplete for a focal tile (i.e., less than eight neighbouring tiles), such as  
254 for tiles along the coastline or at the edge of the covered extent. For those tiles, no slope can be derived for the rows or columns  
255 at the edge of the mosaic. These cells in those rows and columns have no neighbouring cells and *gdaldem* assigns the no data  
256 value (-9999) to these cells. Please also note that we calculated the slope descriptor from the 10 m aggregate of the  
257 DTM/Terrain data set rather than deriving it from the 0.4 m original resolution rasters and then aggregating it. The latter  
258 approach could represent the aspect/slope at the original resolution better (Grohmann, 2015; Moudrý et al., 2019), but would  
259 create inconsistencies within how the remaining DTM/Terrain descriptors are calculated in this dataset.

#### 260 **3.4.4 Landscape openness mean (openness\_mean)**

261 Landscape openness is a landform descriptor that indicates whether a cell is located in a depression or elevation of the  
262 landscape. We calculate the landscape openness following Yokoyama et al. (2002) using the OPALS implemented algorithms.  
263 We used a mean aggregate of the elevation model with 10 m grain size and 32bit floating point precision, and derived the  
264 mean landscape openness for a cell as the mean of the landscape openness in all eight cardinal directions with a search radius  
265 of 150 m. We chose to base this descriptor on the aggregated 10 m elevation model and a 150 m search radius, as we think  
266 that these are best suited to describe the landscape scale variation in the landforms of Denmark. Danish landscapes are  
267 characterised by gently undulating terrain, valleys forged by small to medium sized rivers and dune systems along the  
268 coastlines. First, we generated a mosaic including the focal tile and all available tiles in the direct neighbourhood (max. eight  
269 neighbouring tiles) to reduce edge effects in subsequent calculations. The mean of the positive openness for all eight cardinal  
270 directions with search radius of 150 m was then derived for all cells in the mosaic using the OPALS Openness module (options:  
271 feature = 'positive', kernelSize = 15 and selMode = 0). Next, the mean openness per cell was converted from radians to degrees,  
272 rounded to the nearest integer and stored as a 16-bit integer. For incomplete neighbourhood mosaics (i.e. containing less than  
273 eight neighbouring tiles) we then masked out cells within the first 150 m of all edges where a neighbourhood tile was missing.  
274 Finally, the output was cropped back to the extent of the focal tile. As a consequence of the edge effect related masking, the  
275 focal tiles on the fringes of the data set, such as those on coastlines or at the edge of the coverage area, have no data available  
276 for the first 150 m. The corresponding cells for the affected areas are set to the NODATA value -9999.

#### 277 **3.4.5 Landscape openness difference (openness\_difference)**

278 In addition to the mean of the landscape openness, we also derived a landscape openness difference measure. This difference  
279 measure is an indicator of whether a cell is part of a linear feature in the landscape that runs in one cardinal direction, such as

280 a ridge or valley, therefore providing additional information to the landscape openness\_mean descriptor. We calculated the  
281 landscape openness difference based on the 10 m mean aggregate of the elevation model (32bit floating point precision) and  
282 with a search radius of 50 m. We chose these parameters as we consider them best suited to capture the relatively narrow  
283 valleys and ridgetops common in the Danish landscape. First, we generated a mosaic including the focal tile and all available  
284 tiles in the direct neighbourhood (max. eight neighbouring tiles) to reduce edge effects in subsequent calculations. We then  
285 calculated the minimum and maximum of the positive landscape openness from all eight cardinal directions for all cells in the  
286 mosaic using the OPALS Openness module with a search radius of 50 m (feature = 'positive', kernelSize = 5 , selMode = 1  
287 for minimum and selMode = 2 for maximum). Next, we converted the minimum and maximum values from radian to degrees  
288 and calculated the difference between the maximum and minimum value. We rounded the result to the nearest full degree. For  
289 the cases where the neighbourhood mosaic was incomplete, i.e., containing less than eight neighbouring tiles, we masked out  
290 all cells within the first 50 m of all edges with a missing neighbourhood tile. The final output mosaic was then cropped to the  
291 extent of the focal tile and stored as a 16-bit integer GeoTIFF. As a consequence of the edge effect related masking, focal tiles  
292 on the edges of the data set, such as those on coastlines or at the edge of the coverage area, have no data available for the first  
293 50 m.

#### 294 **3.4.6 Solar Radiation (solar\_radiation)**

295 Incident solar radiation is a key parameter for plant growth as it represents the electromagnetic energy available to plants  
296 required for photosynthesis. However, in the comparatively flat country of Denmark, shading by other vegetation likely exerts  
297 a larger influence on photosynthetic activity than terrain related shading. Here, the impact of incident solar radiation on the  
298 local climate likely plays a more important role for determining plant growth due to its influence on drought/water dynamics  
299 (Moeslund et al., 2019). We estimated the amount of incident solar radiation received per cell (100 m<sup>2</sup>) per year from the slope  
300 and aspect computed as described above. Calculations were implemented using *gdal\_calc*, following equation 3 specified in  
301 McCune and Keon (2002):

302

$$303 \quad solar\_radiation = 10^6 \times e^{0.339+0.808 \times \cos(L) \times \cos(S)-0.196 \times \sin(L) \times \sin(S)-0.482 \times \cos(180 - |(180 - A)|)} \times \sin(S) \quad (1)$$

304 where  $L$  is the centre latitude of the cell in degrees,  $S$  is the slope of the cell in degrees and  $A$  is the aspect of the cell in degrees.  
305 The resulting estimate is given in: MJ x 100<sup>-1</sup> m<sup>-2</sup> x yr<sup>-1</sup> (McCune and Keon, 2002). Slope and aspect for each 10 m x 10 m  
306 grid cell were sourced from the slope and aspect rasters. We saved the result as 32-bit integers. Due to propagation from the  
307 calculation of slope descriptor, no solar radiation values can be calculated for cells found right on the edge of the data set, for  
308 example in tiles situated along the coastline or at the edge of the sampling extent.

### 309 **3.4.7 Heat Load Index (heat\_load\_index)**

310 The heat load index (McCune and Keon, 2002) was originally developed as an indicator for temperature based solely on aspect,  
311 but this characteristic is probably better captured in our solar radiation descriptor (see above) that was developed to improve  
312 shortcomings in the heat load index (McCune and Keon, 2002). However, in a previous study (Moeslund et al., 2019) we show  
313 that - in Denmark - the index was moderately correlated with soil moisture, and can therefore serve as an useful indicator of  
314 the amount of moisture available to plants. We calculated the heat load index based on the aspect rasters (described above)  
315 following the equation specified in McCune and Keon (2002) using *gdal\_calc*:

316

$$heat\_load\_index = \frac{(1 - \cos(A - 45))}{2} \quad (2)$$

317

318 where  $A$  is the aspect in degrees. We stretched the result by a factor of 10000, rounded to the nearest integer and stored it as a  
319 16-bit integer. As the *heat\_load\_index* is not meaningfully defined for flat cells (slope =  $0^\circ$  / aspect =  $-1^\circ$ ), we set the value of  
320 those cells to no data (-9999). Finally, for cells that are located on the outermost edges of the data set the *heat\_load\_index* is  
321 not defined due to propagation of the nodata value assigned to the aspect in those cells.

### 322 **3.4.8 Topographic wetness index (twi)**

323 The topographic wetness index (TWI) provides a proxy measure of soil moisture or wetness based on the hydrological flow  
324 modelled through a digital terrain model. Here, we derived the TWI following the method recommended by Kopecký et al.  
325 (2020). We based our calculations on the aggregated 10 m elevation model (*dtm\_10m*, 16bit integer) and used a neighbourhood  
326 mosaic (max. 8 neighbours) for each focal tile to derive the TWI. The exact procedure is detailed in the next paragraph. As  
327 such the index values calculated by us only consider a catchment the size of one tile and all its neighbours (for non-edge tiles  
328 this is a 3 km x 3 km catchment, for edge tiles it is smaller depending on the completeness of the neighbourhood mosaic). We  
329 then cropped the resulting output back to the extent of the focal tile, stretched the TWI values by a factor of 1000, rounded to  
330 the next full integer and stored the results as a 16-bit integer.

331 We calculated the TWI using SAGA GIS v. 7.8.2 binaries. First, we sink-filled the neighbourhood mosaic of the terrain model  
332 using the *ta\_preprocessor 5* module and the option “MINSLOPE 0.01” (Wang and Liu, 2006). Second, we calculated the flow  
333 accumulation based on the sink-filled neighbourhood mosaic of the terrain model (from step one) using the *ta\_hydrology 0*  
334 module with options “METHOD 4” and “CONVERGENCE 1.0” (Freeman, 1991; Quinn et al., 1991). Third, we derived the  
335 flow width and specific catchment area based on the sink-filled neighbourhood mosaic of the terrain model (from step one)  
336 and the flow accumulation (from step two) using the module *ta\_hydrology 19* (Gruber and Peckahm, 2008; Quinn et al., 1991).  
337 Fourth, we calculated the slope based on the sink-filled neighbourhood mosaic of the terrain model (from step one) using the  
338 *ta\_morphometry 0* module with option “METHOD 7” (Haralick, 1983). Finally, we derived the TWI based on the specific

339 catchment area (from step three) and slope (from step four) using the module `ta_hydrology 20` (Beven and Kirkby, 1979;  
340 Böhner and Selige, 2006; Moore et al., 1991). For detailed descriptions of the modules used, please refer to the SAGA GIS  
341 documentation (SAGA-GIS Tool Library Documentation v7.8.2, 2021).

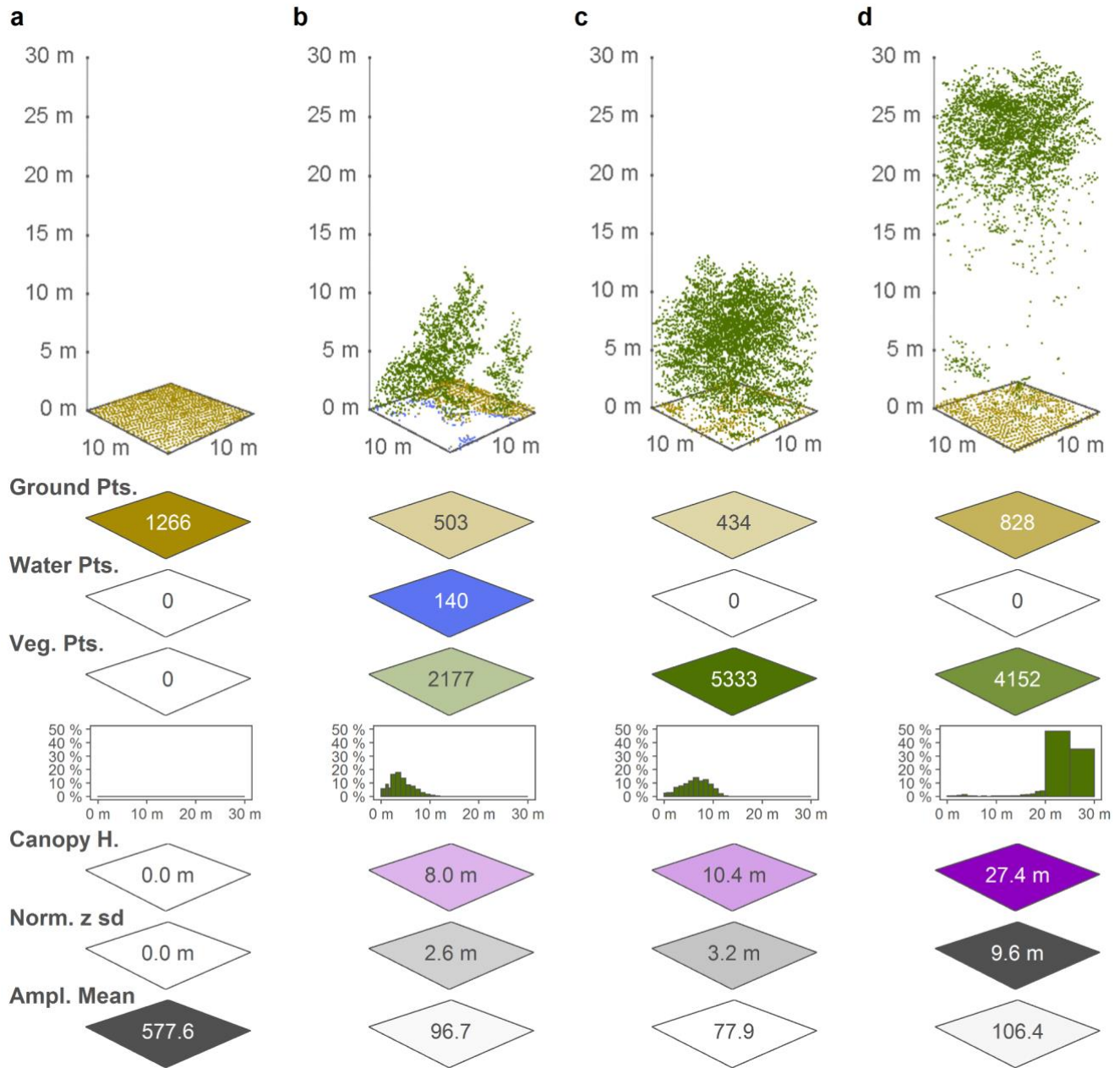
342 The TWI descriptor calculated for EcoDes-DK15 is subject to two main limitations: edge effects and small catchment size.  
343 Tiles with incomplete neighbourhoods (i.e., less than 8 direct neighbours are available) will suffer from edge effects in the  
344 direct vicinity of the relevant border and overall due to a reduced catchment size. Furthermore, even in the ideal case of the  
345 neighbourhood being complete, for most cells flow accumulation is therefore only calculated for the direct neighbourhood of  
346 a focal tile, comprising a 3 km x 3 km catchment area. While we hypothesize that, due to the relatively low variation in  
347 topography in Denmark, the TWI based on this comparably small catchment area will serve as a reasonable proxy for terrain-  
348 based wetness in most cases, it may be less reliable in areas with exceptionally high variation in topography or for lakes and  
349 rivers with large catchments. In addition, we would like to point the reader towards the general limitations of the TWI as a  
350 proxy for soil moisture or terrain wetness as for example discussed by Kopecký et al. (2020). These general limitations should  
351 be taken into account when interpreting the TWI values provided in EcoDes-DK15.

### 352 **3.5 Point-cloud derived descriptors**

353 The DHM/Point-cloud point cloud was pre-classified into eleven point categories (Geodatastyrelsen, 2015) following the  
354 ASPRS LAS 1.3 standard (ASPRS, 2011). For the EcoDes-DK15 data set, we restricted the analysis to six of these classes,  
355 including ground points (“Terræn”) - class 2, water points (“Vand”) - class 9, building points (“Bygninger”) - class 6, as well  
356 as low (“lav”), medium (“mellemhøj”) and high vegetation (“høj vegetation”) - classes 3, 4 and 5, respectively. We grouped  
357 the three vegetation classes into one single vegetation class and, instead of the pre-assigned height categories, considered a  
358 more detailed set of height bins (see point count and proportion descriptions below). The overall classification accuracy of the  
359 point cloud was assessed by the Danish authorities (Flatman et al., 2016), but limited information is available for the accuracy  
360 in each class. Thus, some degree of noise should be assumed across all classes. The tall vegetation category (class 6) was used  
361 as a catch-all class if classification failed, as often the case for very tall buildings and structures (Flatman et al., 2016). To  
362 reduce the noise related to such structures, we removed vegetation points with a normalised height exceeding 50 m above  
363 ground when calculating the vegetation point counts. We included all returns, i.e., first returns and echoes, in our analysis.

364 All point cloud processing was carried out using OPALS and the OPALS Python bindings. As none of the point cloud derived  
365 descriptors required mosaicking to prevent edge-effects, we processed all point cloud descriptors on the focal tile only. After  
366 the initial ingestion of the LAZ-file for a tile into the OPALS data manager format (odm), we used the *OpalsAddInfo* module  
367 to add a normalised height (z) attribute to the points. For this attribute we subtracted the height of the ground derived from the  
368 corresponding DHM/Terrain raster (0.4 m grid size) from the height above sea level of each point. Figure 3 illustrates how the

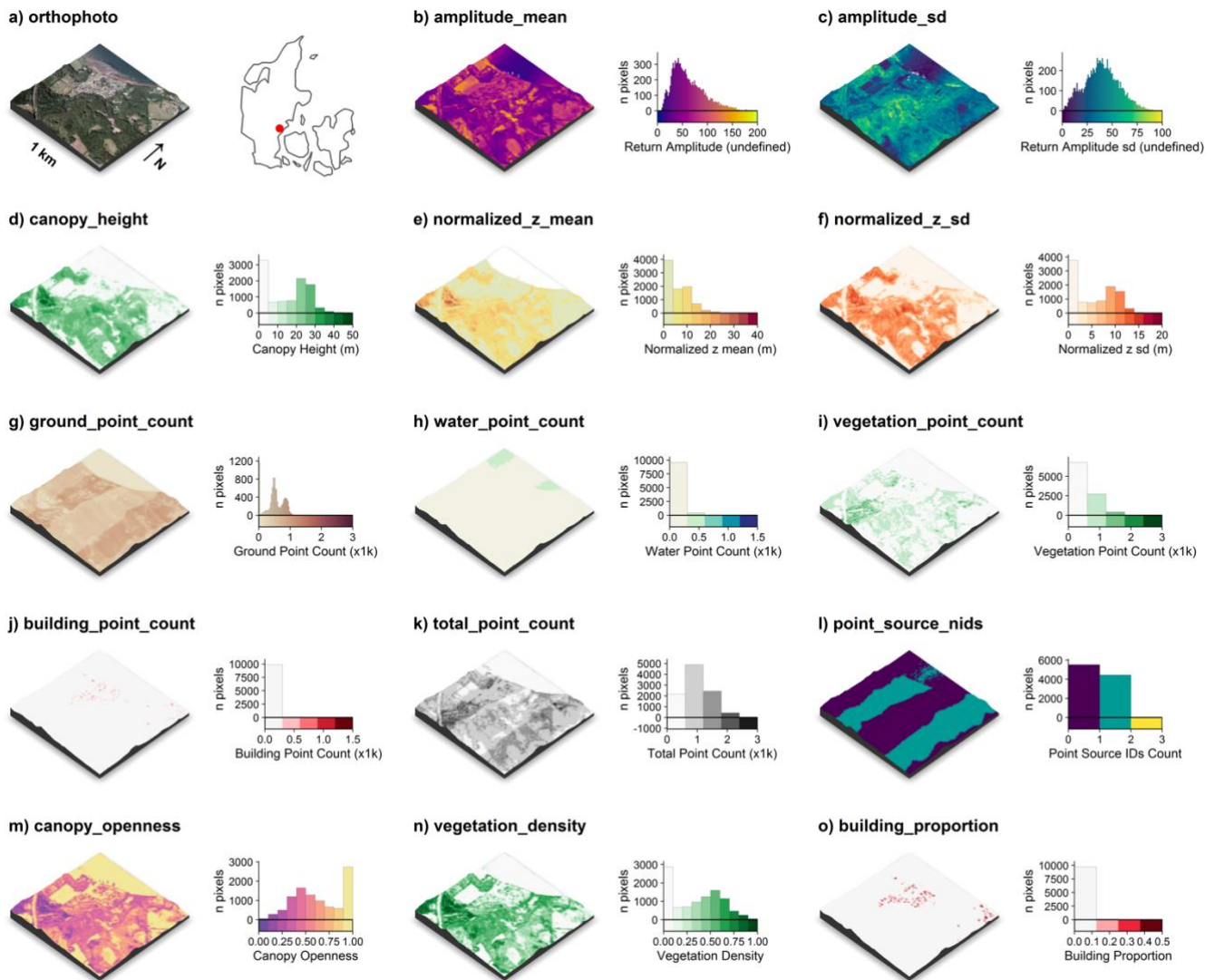
369 point cloud data translates to some of the descriptor outputs for four exemplary 10 m x 10 m cells from the data set, and an  
 370 overview of the point cloud derived descriptors for a 1 km x 1 km tile in Vejle Fjord in central Jutland is provided in Fig. 4.



371  
 372 **Figure 3:** Point cloud examples for four 10 m x 10 m cells and a selection of the associated EcoDes-DK15 descriptors derived  
 373 from the point clouds, illustrating the ecological meaning and some of the limitations of the EcoDes-DK15 data set. The 10 m  
 374 x 10 m cells represent the following environments: a) an agricultural field, b) the edge of a forest / parkland pond with low  
 375 vegetation, c) a young plantation of dense coniferous trees, and d) old growth mixed-woodland. The EcoDes-DK15 descriptors



376 shown include (from the top) the total point counts for each cell in the three main EcoDes-DK15 categories: 1) the number of  
377 returns classified as ground, 2) the number of returns classified as water and 3) the number of returns classified as vegetation.  
378 In addition, the relative proportion of vegetation points per predefined height bin is illustrated below the total vegetation point  
379 count. Finally, the bottom three panels show the estimated canopy height (altitude above ground for the 95%-percentile of all  
380 vegetation returns), the normalized z standard deviation (variation in height above ground for all return classes), and the mean  
381 return amplitude for each cell. Please note how the classification of the point cloud classification does not separate between  
382 very low growing vegetation (e.g., grass) and ground points in the agricultural field shown in a), and how returns from water  
383 are only registered in shallow areas close to the water bodies edge, such as exemplified by the forest pond in b). Lastly, we  
384 would like to point the reader to the general limitations of ALS in penetrating forest canopies such as those shown in c) and  
385 d). While the upper layers of the canopies are well resolved in both cases, the laser scanning struggles to capture some aspects  
386 of the lower layers; the ground returns were frequently blocked by the thick canopy in c) and the laser fails to meaningfully  
387 characterise understory vegetation and stems in d).  
388



389

390 **Figure 4:** Illustration of the point cloud derived descriptors for a 1 km x 1 km tile along Vejle Fjord (tile id: 6171\_541). An  
 391 orthophoto and the tile location relative to Denmark are shown in (a). The point cloud derived descriptors comprise of: c) the  
 392 mean return amplitude, d) the standard deviation in the return amplitude, e) the canopy height (vegetation returns only), f) the  
 393 mean of the normalized height above ground (all returns), g) the mean of the normalized height (all returns), h) the ground  
 394 point count, i) the water point count, j) the building point count, k) the total point count, l) the number of point sources (flight  
 395 strips), m) the canopy openness, n) the vegetation density and o) the building proportion. Note the influence of point source  
 396 overlap illustrated in l) on some of the descriptors, for example: g) ground point count, i) vegetation point count and k) total  
 397 point count (see Sect. 3.5.5 for detail). For visualisation purposes, we amplified the altitude above sea-level by a factor of two  
 398 in the 3D visualisations and divided the point counts by 1000. The 3D raster visualisations were generated using the rayshader

399 v0.19.2 package in R (Morgan-Wall, 2020). Orthophotograph provided by the Danish Agency for Data Supply and Efficiency  
400 (<https://sdfe.dk/hent-data/fotos-og-geodanmark-data/>).

### 401 **3.5.1 Amplitude – mean and standard deviation (amplitude\_mean and amplitude\_sd)**

402 The amplitude attribute of a point in the DHM/Point-cloud is the actual amplitude of the return echoes, i.e., it describes the  
403 strength of the LiDAR return signals detected by the sensor. The descriptor is difficult to interpret in terms of its ecological  
404 meaning. Nonetheless, we believe that it is still useful for vegetation classifications, biodiversity analysis and other applications  
405 that perform well with proxy data. We calculate the arithmetic mean and standard deviation of the amplitude for all points  
406 within a 10 m x 10 m cell. Here, ‘all points’ refers to all points classified as ground, water, building, and vegetation points.  
407 Calculations were carried using the *OPALS Cell* module and results were stored as 32-bit floats. The amplitude attributes in  
408 the DHM/Point-cloud point clouds are not directly comparable when points originate from different point sources (e.g., flight  
409 strips), as the amplitude has not been calibrated and hence is sensitive to differences in sensor, sensor configuration and signal  
410 processing. Calculating summary metrics such as mean and standard deviation for a 10 m x 10 m cell where points from  
411 different point sources are present introduces additional complexities. In some cases, a 10 m cell might contain points from up  
412 to four different sources. We therefore recommend using the two amplitude descriptors with care, and - if possible - in  
413 conjunction with information on the point source ids contained in the point\_source\_info descriptors described below.

### 414 **3.5.3 Canopy height (canopy\_height)**

415 Canopy height is a key parameter of vegetation structure related to biomass and ecosystem functioning. We derived the canopy  
416 height in metres as the 95th-percentile of the normalised height above ground of all vegetation points within each 10 m x 10  
417 m cell using the *OPALS Cell* module. The resulting canopy heights were multiplied by a factor of 100, rounded to the nearest  
418 integer and stored as 16-bit integers. In cases where there were no vegetation points in any given cell, we set the canopy height  
419 value of the cell to zero metres. Please note that the canopy height is therefore also set as zero metres even if there are no points  
420 present in the cell at all (such as ground or water points). Furthermore, our algorithm calculates the canopy height even if there  
421 is only a small amount of vegetation points in a cell. In rare cases, this might lead to erroneous canopy-height readings if  
422 vegetation is found on artificial structures or points have been mis-classified. For example: A tall communications tower can  
423 be found just south of Aarhus and returns from the tower were miss-classified as vegetation. The resulting canopy height for  
424 this cell is calculated as > 100 m above ground, which would not make sense if interpreted as a height of the vegetation above  
425 ground. For such cases, the building proportion descriptor may be used to separate cells with artificial structure from those  
426 with vegetation only. See also the “normalized\_z” descriptor below for a closely related measure.

### 427 **3.5.4 Normalised height - mean and standard deviation (normalized\_z\_mean and normalized\_z\_sd)**

428 Similar to the canopy height descriptor, the normalised height describes the structure properties of the point cloud above  
429 ground. The key difference between the two descriptors is that for the normalised height we also included non-vegetation

430 points (buildings & ground) and derived the summary statistic as the mean rather than the 95%-quantile. For the normalised  
 431 height descriptor, we also provide a measure of variation in form of the standard deviation. Specifically, we calculated the  
 432 normalised mean and the standard deviation of the mean height above ground (normalised z attribute) for all points in each 10  
 433 m x 10 m grid cell using the *OPALS Cell* module. The results were multiplied by 100, rounded to the nearest integer and stored  
 434 as 16-bit integers. We used the normalised z attribute generated during the ingestion of the point cloud reflecting the height of  
 435 a point relative to the ground level determined by the DHM/Terrain raster. Here, all points refer to all points belonging either  
 436 to the ground, water, building or vegetation class. By definition the normalised height mean will be highly correlated with the  
 437 “canopy\_height” descriptor for cells where mainly vegetation points are present. We kept the American spelling of the  
 438 descriptor name for legacy reasons with previous versions of the data set.

### 439 3.5.5 Point counts (xxx\_point\_count\_xxx)

440 The point count descriptors are intermediate descriptors used to generate the proportion descriptors described below. However,  
 441 they can also be used to calculate tailored proportion descriptors relevant to addressing a specific ecological objective (see  
 442 use-case example in Sect. 4.2). For EcoDes-DK15 we derived thirty point count descriptors for each 10 m x 10 m cell based  
 443 on filtering of the pre-defined point classifications and separation by height above ground (normalised z) using the *OPALS*  
 444 *Cell* module. All point counts were stored as 16-bit integers. These thirty descriptors contain six general point counts, including  
 445 ground, water, vegetation, building and total point counts (Table 3), as well as twenty-four vegetation point counts separated  
 446 in height bins (Table 4). Note that the number of returns within a 10 m cell is influenced by a) the number of point sources  
 447 present in the cell, b) the relative position and distance of a cell to the point source when the data was collected (i.e., to the  
 448 flight path), and c) by the point source themselves (i.e., differences between the LiDAR sensors deployed). The absolute counts  
 449 are therefore not directly comparable between cells and need to be standardised first, for example by division of the total  
 450 number of point counts as done for the point proportion descriptors derived by us.

451  
 452 **Table 3:** General point count descriptors, as well as the height ranges and point classes included in each descriptor.  
 453

Descriptor name	Height range	Point classes
ground_point_count_-01m-01m	-1 m to 1 m	ground points (class 2)
water_point_count_-01m-01m	-1 m to 1 m	water points (class 9)
ground_and_water_point_count_-01m-01m	-1 m to 1 m	ground and water points (classes 2,9)
vegetation_point_count_00m-50m	0 m to 50 m	vegetation points (classes 3,4,5)
building_point_count_-01m-50m	-1 m to 50 m	building points (class 6)
total_point_count_-01m-50m	-1 m to 50 m	ground, water, vegetation and building points (classes 2,3,4,5,6,9)

454

455 **Table 4:** Vegetation point count descriptors divided into twenty-four height bins. All vegetation point counts include the point  
 456 classes 3,4 and 5.  
 457

<b>Descriptor name</b>	<b>Height range</b>
vegetation_point_count_00.0m-00.5m	0.0 m to 0.5 m
vegetation_point_count_00.5m-01.0m	0.5 m to 1.0 m
vegetation_point_count_01.0m-01.5m	1.0 m to 1.5 m
vegetation_point_count_01.5m-02.0m	1.5 m to 2.0 m
vegetation_point_count_02m-03m	2 m to 3 m
vegetation_point_count_03m-04m	3 m to 4 m
vegetation_point_count_04m-05m	4 m to 5 m
vegetation_point_count_05m-06m	5 m to 6 m
vegetation_point_count_06m-07m	6 m to 7 m
vegetation_point_count_07m-08m	7 m to 8 m
vegetation_point_count_08m-09m	8 m to 9 m
vegetation_point_count_09m-10m	9 m to 10 m
vegetation_point_count_10m-11m	10 m to 11 m
vegetation_point_count_11m-12m	11 m to 12 m
vegetation_point_count_12m-13m	12 m to 13 m
vegetation_point_count_13m-14m	13 m to 14 m
vegetation_point_count_14m-15m	14 m to 14 m
vegetation_point_count_15m-16m	15 m to 16 m
vegetation_point_count_16m-17m	16 m to 17 m
vegetation_point_count_17m-18m	17 m to 18 m
vegetation_point_count_18m-19m	18 m to 19 m
vegetation_point_count_19m-20m	19 m to 20 m
vegetation_point_count_20m-25m	20 m to 25 m
vegetation_point_count_25m-50m	25 m to 50 m

### 458 **3.5.6 Vegetation proportions by height bin (vegetation\_proportion\_XXX)**

459 The vegetation proportions by height bin are amongst the key parameters in the EcoDes-DK15 data set describing vegetation  
460 structure as they provide an indication of how the vegetation is distributed vertically within each cell of the raster. We  
461 calculated the proportions by dividing the vegetation count for each height bin (Table 4) by the total point count  
462 (total\_point\_count\_-01m-50m) within a given 10 m x 10 m cell. Resulting proportions were multiplied by a factor of 10000,  
463 rounded to the nearest integer and converted to 16-bit integers. All calculations were done using *gdal\_calc* based on the  
464 respective point count rasters (Sect. 3.3.5). The naming convention of the vegetation proportion descriptors  
465 “vegetation\_proportion\_XXX” follows the same convention as the vegetation point count descriptors (Table 4), whereby the  
466 suffix “XXX” is replaced with the respective height bin. Please note that height bins are spaced at 0.5 m intervals below 2 m  
467 and at 1 m intervals between 2 m and 20 m. Furthermore, the range above 20 m is split into only 2 bins: 20 m to 25 m and 25  
468 m to 50 m.

469 Given the properties of the DHM/Point-cloud we recommend being cautious when interpreting differences in the lower height  
470 bins. It is likely that the inaccuracies in the point cloud complicate clear separation between points less than half a metre apart.  
471 Furthermore, note that the proportions in the 0 m - 0.5 m bin are likely biased towards an underrepresentation of the vegetation  
472 proportion in this height bin, due to challenges in separating vegetation from ground points during the pre-classification. Lastly,  
473 keep in mind that dense canopy layers in the upper story of the canopy will reduce penetration of the light beam to the lower  
474 canopy layers. This may result in few returns in the lower layers (for example Fig 3 d) even though perhaps vegetation is  
475 present in those layers.

### 476 **3.5.7 Vegetation density or total vegetation proportion (vegetation\_density)**

477 Vegetation density is an important component of ecosystem structure. Here, we calculated the vegetation density as the ratio  
478 between the vegetation returns across all vertical height bins (vegetation\_point\_count\_00m-50m) and the total point count  
479 (total\_point\_count\_-01m-50m). Calculations were done using *gdal\_calc* based on the two point count rasters (Sect. 3.3.5).  
480 Results were multiplied by 10000, rounded to the nearest integer and stored as 16-bit integers. In addition to actual difference  
481 between vegetation density in a cell, the vegetation\_density descriptor is also influenced by the canopy properties, e.g. a dense  
482 upper layer will prevent penetration of the light beam to lower layers or even the ground, and the points sources within a cell,  
483 e.g. multiple sources from different viewing angles provide a more complete estimate of the vegetation density. These  
484 additional influences are important to keep in mind when interpreting the vegetation\_density descriptor.

### 485 **3.5.7 Canopy openness, or ground and water proportion (canopy\_openness)**

486 Canopy openness is an important ecological descriptor particularly of forest canopies, as it describes the amount of light  
487 penetrating through to the levels of the canopy. To some degree the canopy openness serves as the inverse for the vegetation  
488 density. For EcoDes-DK15, we calculated the canopy openness of a 10 m x 10 m cell as the proportion of the ground and water

489 points (ground\_and\_water\_point\_count\_-01m-01m) to the total point count (total\_point\_count\_-01m-50m) within the cell.  
490 The raster calculations were done using *gdal\_calc*. Results were multiplied by 10000, rounded to the nearest integer and stored  
491 as 16-bit integers. Please note that the same considerations as for the vegetation\_density descriptor (Sect. 3.3.7) regarding  
492 canopy properties and differences in point sources between the cells apply when interpreting the canopy\_openness descriptor.  
493 In addition, it is important to note that building points will reduce the canopy openness the same way that vegetation points  
494 would.

### 495 **3.5.8 Building proportion (building\_proportion)**

496 In a densely populated country such as Denmark, buildings form an important part of the landscape. For ecological studies the  
497 distance to buildings, their presence, absence or density may be of relevance. The building\_proportion descriptor of EcoDes-  
498 DK15 provides a proxy for how much building infrastructure can be found within a 10 m cell. We calculated the descriptor as  
499 the number of building points (building\_point\_count\_-01m-50m) divided by the total number of points (total\_point\_count\_-  
500 01m-50m) within each cell using *gdal\_calc*. Results were multiplied by 10000, rounded to the nearest integer and stored as  
501 16-bit integers. While most returns from three dimensional infrastructure are classified as buildings in the DHM/Point-cloud,  
502 we would like to highlight that many roads are classified as ground (class 2) and some structures such as pylons and power  
503 lines were assigned a separate class (not described in (Geodatastyrelsen, 2015)). These structures are therefore not included in  
504 the building\_proportion descriptor. We would further like to note that the majority of building points are likely based on returns  
505 from the roofs of the buildings. Walls and other vertical structures are probably represented at a lower frequency in the point  
506 clouds. Finally, we would like to point the reader to the “DCE Basemap” (Levin, 2019) which may assist in the identification  
507 of basic land cover types that include buildings and other manmade structures.

## 508 **3.6 Auxiliary data**

509 In addition to the terrain and point cloud derived descriptors we provide three sets of auxiliary data with EcoDes-DK15. These  
510 are four layers of ALS point source information, a mask for inland water and a sea mask, as well as a shapefile of the footprints  
511 of the 1 km x 1 km tiles in the data set and their unique identifier.

### 512 **3.6.1 Point source information**

513 The point source attribute of the DHM/Point-cloud represents differences between sensor units or aircrafts that may have been  
514 used during the nationwide LiDAR campaign, differences in the acquisition time and date and differences in the viewpoint or  
515 acquisition angle of the cells. To aid in interpretation of descriptors that may be particularly influenced by point source, like  
516 the amplitude descriptors or the vegetation proportions, we provide summary information about the point sources within each  
517 10 m x 10 m cell. We summarised this information in four descriptors, the “point\_source\_counts”, “point\_source\_ids”,  
518 “point\_source\_nids” and “point\_source\_proportions”. For each tile (file name suffix = tile id), these descriptors are found in  
519 four subfolders bundled up in the parent “point\_source\_info” folder.

520 **point\_source\_ids** - Multi-layer raster containing one 16-bit integer layer for each point source id found in a tile. If a point  
521 with a given point source id is present the value of the cell is set to the point source id (an integer number) in the respective  
522 layer for the point source id, otherwise the value of a cell is set to 0. This multilayer raster can be used to match the file names  
523 of the `point_source_counts` and `point_source_proportions` rasters to a given point source id. Point source ids were extracted  
524 using *Opals Cell*.

525 **point\_source\_nids** - Single layer GeoTiff files containing the number of different point source ids in each cell stored as 16-  
526 bit integers. We calculated the number of point source ids based on the `point_source_ids` descriptor using *gdal\_calc*.

527 **point\_source\_counts** - For each tile there are multiple rasters (up to four), one raster for each point source id found in the  
528 point cloud of the tile (see the *point\_source\_ids* descriptor). These rasters are named with an additional suffix, which matches  
529 the integer point source id for which the point counts are given in the raster (e.g. `point_source_counts_xxxx_xxx_y*`, where  
530 `xxxx_xxx` is the tile id and `y*` the integer point source id). The rasters contain the number of points per 10 m x 10 m cell for  
531 the respective point source id in the tile. Counts were extracted using the *OPALS Cell* module and stored as 16-bit integers.

532 **point\_source\_proportions** - For each tile there are multiple rasters (up to four), one raster for each point source id found in  
533 the point cloud of the tile (see the *point\_source\_ids* descriptor). These rasters are named with an additional suffix, which  
534 matches the integer point source id for which the point proportions are given in the raster (e.g.  
535 `point_source_proportions_xxxx_xxx_y*`, where `xxxx_xxx` is the tile id and `y*` the integer point source id). Each raster contains  
536 the proportion of the point counts for a given point source id in relation to the total point count per 10 m x 10 m cell.  
537 Calculations were carried out using *gdal\_calc*. The final proportions were multiplied by a factor of 10000, rounded to the  
538 nearest integer and stored as 16-bit integers.

### 539 **3.6.2 Water masks (inland\_water\_mask and sea\_mask)**

540 We also provide rasterized water masks for use cases that require masking inland water bodies or the sea. To represent all  
541 permanent lakes in Denmark, we merged three shapefiles containing (1) lakes protected by the Danish nature protection  
542 legislation (§3, available at <https://arealinformation.miljoportal.dk>), (2) other valuable lakes (available on request at the  
543 Danish Farming Agency in the “good farming and environmental condition” data set) and (3) a layer containing the remaining  
544 rather small lakes and ponds (GeoDanmark, <https://kortforsyningen.dk/>). The combined shapefile is provided on the GitHub  
545 code repository (see below). We then burned the geometries within the shapefile into the 10 m x 10 m grid using *gdal\_rasterize*.  
546 The masks are binary, a cell value of 1 indicates land and a value of -9999 (no data) indicates sea or inland water, respectively.  
547 When using the masks please consider that the shape, presence and absence of water bodies and coastlines may fluctuate over  
548 time. We created the masks to present a snapshot of the water bodies as close as possible to the time point of the DHM/Point-  
549 cloud acquisition (spring 2014 - summer 2015), but inaccuracies may still arise. When combining the data with more recent  
550 observations, keep in mind that inland water bodies and coastlines may have changed since then. Finally, while we aimed to



551 produce the inland water mask to be as comprehensive as possible, some small ponds and water bodies may have been missed.  
552 Note also that while some rivers are included in the sea mask, the inland water mask does not include rivers or streams. The  
553 masks can be found in the “masks” subfolder of the complete data set.

### 554 **3.6.3 Vegetation point date stamps (date\_stamp\_min, date\_stamp\_max, date\_stamp\_mode)**

555 The time point at which the source data was collected may be of interest to certain applications that are using EcoDes-DK15  
556 vegetation descriptors. These include for example, comparisons amongst regions where the data was collected under different  
557 foliage conditions (leaf-on/leaf-off) or studies that require a precise timing of the sample such as change detection studies. To  
558 better facilitate these applications, we generated three date\_stamp descriptors that summarize the GPS time stamps of the  
559 vegetation points within each 10 m x 10 m cell. The three descriptors are: date\_stamp\_min, date\_stamp\_max and  
560 date\_stamp\_mode, which represent the earliest, latest and most common survey date for the vegetation points in any given cell  
561 in the format “YYYYMMDD”, where YYYY is the year in four digits, MM the month in two digits and DD the day in two  
562 digits.

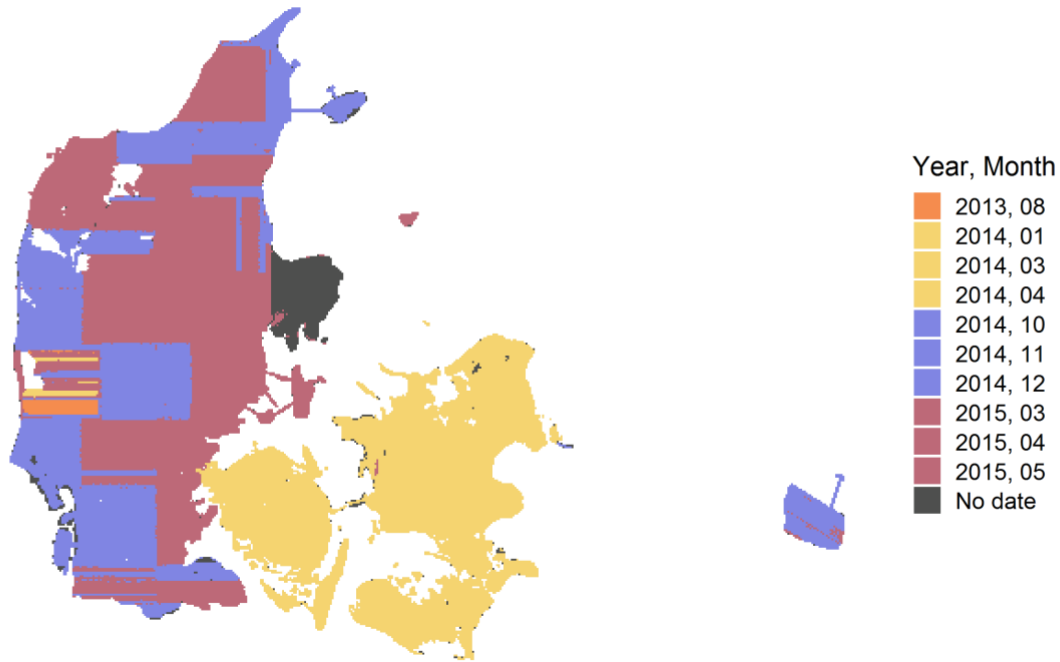
563 We used the *OPALS addInfo* module to generate a new “GPSTime” attribute for all vegetations points (classes 3,4,5) by dividing  
564 the GPSTime (seconds since 6 January 1980) attribute by 86400 (seconds per day) and taking the floor value of the result. We  
565 then exported the min, max and mode for each 10 m x 10 m cell using the *OPALS Cell* module, loaded the output rasters into  
566 Python and converted the \_GPSTime values into year, month and day in CET using the *datetime* module. Finally, we exported  
567 the min, max and mode dates as 32bit integers.

568 Note that the date\_stamp descriptors only cover points that are classified as vegetation and therefore do not provide information  
569 about the time point at which points belonging to other classes were surveyed (e.g., ground point, building points etc). We  
570 chose to not include other point classes in the date\_stamp descriptors, as we are aware that all versions of the source data sets  
571 include some ground points from 2007, and as we believe that clear information about the vegetation points is most relevant  
572 for the end-users conducting ecological research. Furthermore, determining the date\_stamps was not possible for a proportion  
573 of tiles where the GPSTime in the source data was not converted from seconds per GPS week to GPS time in seconds since 6  
574 January 1980. A post-hoc conversion is not possible without the knowledge of the exact GPS week number, which is not  
575 provided in the source data. In these cases, we assigned the no data value to the date\_stamps. The majority of the tiles affected  
576 is located in the areas around Mols Bjerge and Sønderborg (Fig. 5). However, from auxiliary information about the source data  
577 sets we know that these areas were surveyed April-May 2015 and October 2014, respectively.

578

## EcoDes-DK15 Vegetation Point Collection Dates

Aggregate of date\_stamp\_mode for each tile



579

580 **Figure 5:** Distribution of the most common survey date for the vegetation points in each tile of the EcoDes-DK15 dataset. The  
581 data shown is aggregated for each tile from date\_stamp\_mode descriptor. The figure highlights that while the majority of the  
582 vegetation points is from 2014/15, the data set also includes a small amount of vegetation points from 2013 in western Jutland.  
583 Furthermore, surveys were conducted in all seasons, with vegetation points originating in spring, summer, autumn and winter.  
584 Nonetheless, the majority of vegetation points comes from the leaf-off season. Lastly, the date\_stamp descriptors could not be  
585 derived for some regions as the GPSTime was not provided in the point clouds. However, from auxiliary information we know  
586 that the surveys in the Mols Bjerger and Sønderborg areas were conducted in April-May 2015 and October 2014, respectively.

### 587 3.6.4 Footprint file (tile\_footprints.shp)

588 To assist data access and creation of data subsets, we have produced an ESRI shapefile containing the footprints of all 1 km x  
589 1 km tiles in the EcoDes-DK15 data set. The shapefile was generated based on the “dtm\_10m” rasters and the tile identifier of  
590 each footprint geometry is specified in the “tile\_id” attribute column.

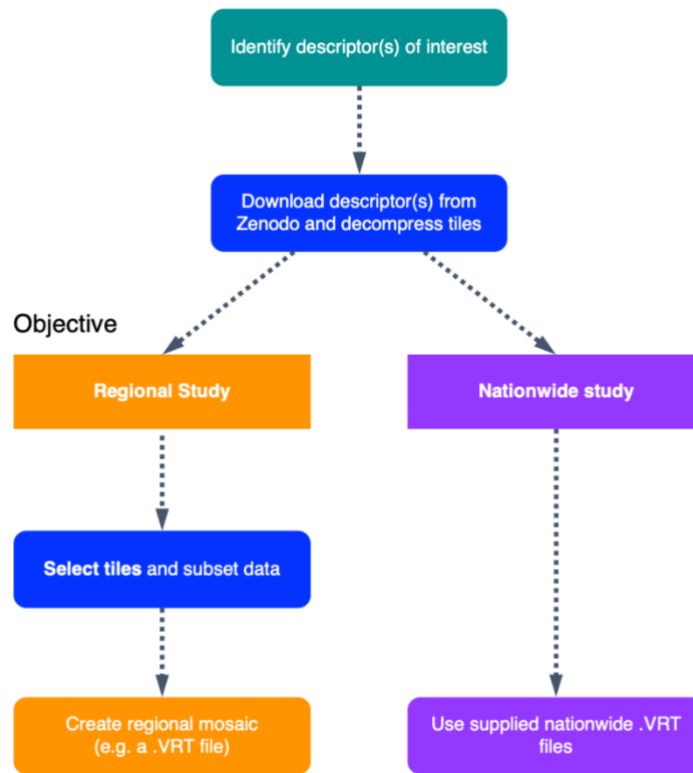
## 591 **4. Data access and ecological use case example**

### 592 **4.1 Data access and handling**

593 Depending on the extent of the study, it may be preferable to work with a subset of the data set rather than the nationwide VRT  
594 files (Fig. 6). We suggest starting by identifying the relevant EcoDes-DK15 descriptors of interest, then retrieving the relevant  
595 data from the repository and decompressing the archives (instructions provided on data repository). If the study area of interest  
596 covers a large fraction of Denmark's extent and sufficient processing power is available, the nationwide VRT data should  
597 provide the most convenient access to the selected descriptors. However, if the study area does not cover a large proportion of  
598 Denmark, then we suggest sub setting the data using the tile footprints to decrease demands on computational resources. After  
599 sub setting, local / regional VRT files or mosaics can be generated if needed. We provide an example R script illustrating how  
600 this sub setting could be done for the use case example shown in the next section on the code repository  
601 ([manuscript/figure 7/subset\\_data set.R](#)). We have also made the resulting subset available as a “teaser” (5 MB) to help the  
602 reader assess the value of EcoDes-DK15 without having to commit to the multi-gigabyte download of the complete data set  
603 (see Sect. 6).

604

## Data access

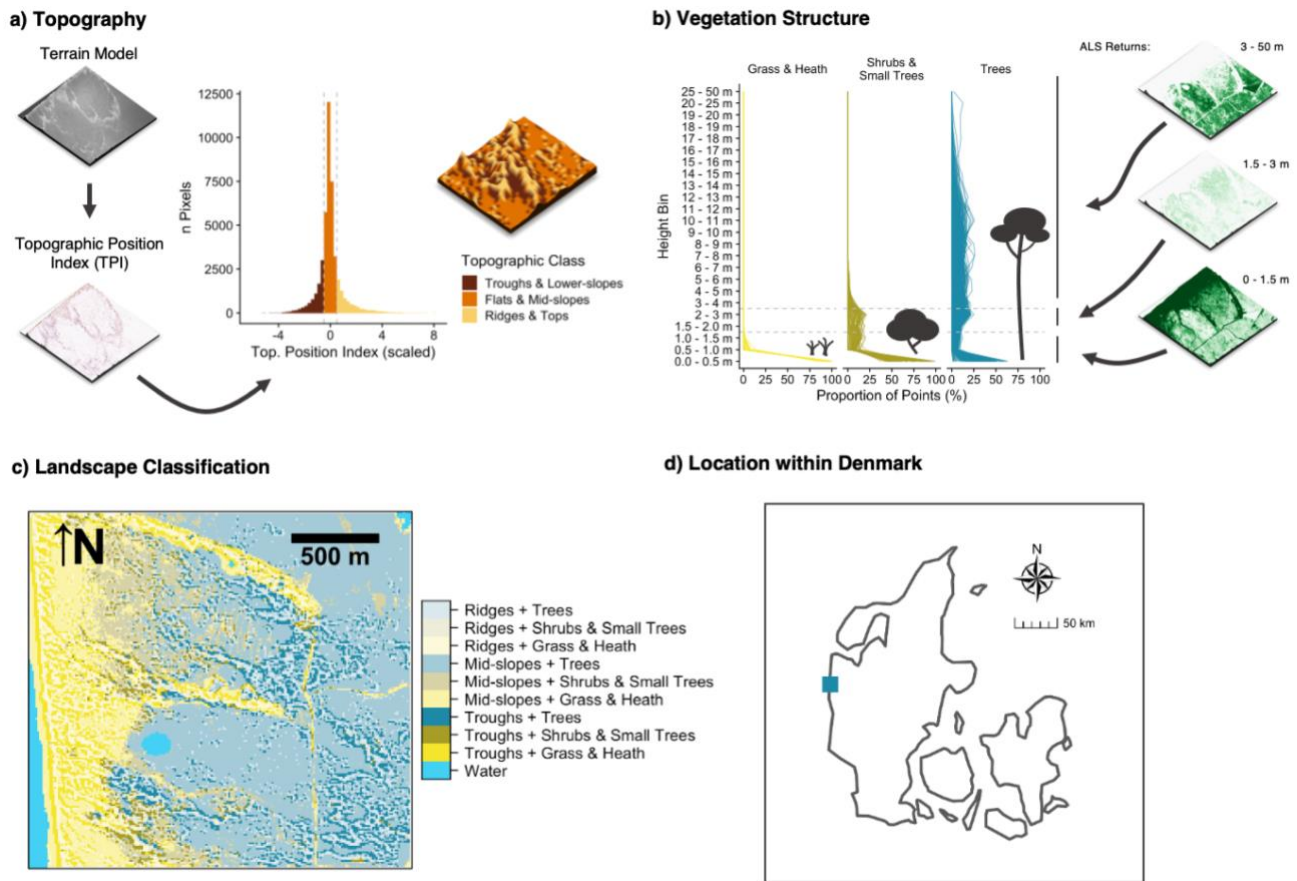


605

606 **Figure 6:** Schematic chart of two possible approaches for accessing and integrating EcoDes-DK15 data into ecological studies.  
607 The first step is to identify which descriptors are of interest, these descriptors can then be downloaded from the Zenodo  
608 repository and decompressed. Next a decision needs to be made whether the whole data set (nationwide) or only a subset of  
609 the tiles is required (e.g., a regional study). As the whole data set is relatively large (~94 GB), storage and processing limitations  
610 need to be taken into account when planning data processing and handling. If a subset of tiles is sufficient for a study, the  
611 provided tile footprints can be used to identify which tiles are required based on a geometry (e.g., a shapefile) of the study  
612 region(s). Finally, for easy data handling in subsequent analysis, a mosaic of the selected tiles can be created. For nationwide  
613 use we provided virtual mosaics (VRT files) containing all tiles for the descriptors. An R script illustrating how the sub setting  
614 can be done for a regional study can be found on the GitHub repository: [https://github.com/jakobjassmann/ecodes-dk-](https://github.com/jakobjassmann/ecodes-dk-lidar/blob/master/manuscript/figure_7/subset_dataset.R)  
615 [lidar/blob/master/manuscript/figure\\_7/subset\\_dataset.R](https://github.com/jakobjassmann/ecodes-dk-lidar/blob/master/manuscript/figure_7/subset_dataset.R).

616 **4.2 Use case example - ecological landscape stratification of Husby Klit nature protected area**

617 Figure 7 illustrates a use case for the EcoDes-DK15 data set with an example of an ecologically motivated landscape  
618 stratification of the “Husby Klit” old-dune protected area in western Denmark. We developed this stratification for a group of  
619 Master’s projects carrying out vegetation monitoring in the area. Our aim was to capture the variation in the dominant  
620 vegetation based on vegetation structure as well as the variation in fine-scale topography created by the dune systems across  
621 the landscape. In addition to using the descriptors already provided, the stratification required us to derive a topographic  
622 position index as well as grouping the point densities in height bins relevant to the characteristics of the three most common  
623 dominant vegetation types (grass and heath, *Pinus mugo* Turra, *Pinus sylvestris* L.) in the area. The source code for this figure  
624 contained in the code repository provides an example of how this can be achieved ([manuscript/figure 7/figure 7.R](#)).  
625



626  
627 **Figure 7:** Use-case example: Landscape stratification of the Husby Klit protected area based on EcoDes-DK15 derived terrain  
628 and vegetation structure descriptors. The target was to stratify the landscape of the Husby Klit “dune plantation” area in the  
629 west of Denmark (56.2837 - 56.3024 °N, 8.1239 - 8.1600 °E) to facilitate stratified random sampling for vegetation monitoring.

630 We identified the four tiles overlapping with the boundaries of the protected area and derived a stratification based on two  
631 components: topographic position (a) and vegetation structure (b). We hypothesized that both components would influence  
632 the vegetation communities present. For the topographic position (a), we first derived and standardised the topographic position  
633 index (TPI) (Weiss, 2001) from the terrain model (dtm\_10m). Following (Weiss, 2001) we then classified each cell based on  
634 the scaled TPI into three categories. A scaled TPI below a value of -0.5 was classified as a “trough or lower-slope”, a scaled  
635 TPI between -0.5 and 0.5 as “mid-slope or flat”, and a scaled TPI above 0.5 as a “ridge or top”. For the vegetation structure  
636 component (b), we calculated the proportion of returns in three simplified height bins: 1) 0 m to 1.5 m, 2) 1.5 m to 3.0 m and  
637 3) 3.0 m - 50 m. Here we included both ground and vegetation returns as the divisor for the standardisation, but not the returns  
638 from buildings or water. Based on *a priori* knowledge we deduced that there are three dominant vegetation communities within  
639 the protected area: communities dominated by grass and heath with vegetation growth generally below 1.5 m, communities  
640 dominated by shrubs and small trees (including the invasive *Pinus mugo*) with vegetation growth predominantly below 3.0 m,  
641 and communities dominated by trees (including the native *Pinus sylvestris*), generally with growth above 3.0 m. We used this  
642 knowledge to assign the three vegetation classes based on the proportion of point returns in the simplified height bins. For the  
643 “grass and heath” class we used a strict cut off with no points present above 1.5 m. For the “shrubs and small trees” class we  
644 used a fuzzy cut off allowing the proportion of points in the 3.0 m and above bin to reach up to 10% of the maximum proportion  
645 found in this height bin. All remaining cells were then assigned to the “trees” class. Finally, we combined the two classifications  
646 into one as illustrated in c). Panel d) shows the location of the protected area within Denmark. The 3D raster visualisations  
647 were generated using the rayshader v0.19.2 package in R (Morgan-Wall, 2020).

## 648 **5. Discussion - limitations and future perspectives**

649 Our data set demonstrates how the complex information in ALS point cloud data sets spanning more than 40.000 km<sup>2</sup>, can be  
650 condensed into a compact data set of rasterized descriptors of interest for ecological studies. For the whole of Denmark, we  
651 provide 70 raster layers representing eighteen measures that describe a snapshot of vegetation height, structure and density, as  
652 well as topography and topography-derived habitat characteristics, including slope, aspect, solar radiation and wetness for the  
653 time period 2014-2015. These measures are of direct relevance for ecological research on species’ habitat characteristics,  
654 distribution modelling, biodiversity and conservation applications. Condensing the ALS derived information into a compact  
655 set of raster descriptors makes it more accessible to the community of ecological researchers and practitioners, allowing them  
656 to access information on the vertical structure of vegetation and terrain otherwise difficult to obtain for large extents such as  
657 those of a whole country.

658 We would like to highlight some key ecological and physical limitations that should be kept in mind when using the data or  
659 derivatives. Firstly, we were able to only carry out a simple qualitative assessment of the errors in the EcoDes-DK14 data set  
660 within the scope of this project. All descriptors should therefore be seen as proxies for the geographical and biological

661 properties they describe. Errors in the original point cloud and DTM will have propagated through to the final descriptors and  
662 future studies are needed to assess to which degree the proxy measures correlate with in-field data. Furthermore, the EcoDes  
663 data set is a snapshot in time representing the state of the vegetation in the one and a half years between spring 2014 and  
664 summer 2015 (with some exception in western Jutland, where the data is from 2013). Like anywhere on Earth, the landscapes  
665 of Denmark may change over time and by the time point of publication of this data set over 5 years may have passed since the  
666 collection of the source data. External data sources containing information about on-going or past changes (such as satellite  
667 imagery - see below) might help overcome this bias. Additionally, the geographical differences in the timing of the point cloud  
668 collection across the country (see Sect 6.3.4) may introduce noise and could affect cross-comparability of the data between  
669 regions, for example due to seasonal differences in foliage (see e.g., Leiterer et al., 2015). Furthermore, there are implicit  
670 limitations in spatial scale due to the set grain size of the data set. We chose a 10 m x 10 m grid for efficiency in computation  
671 and data handling, as well as to overcome limitations in the density of the source point cloud (four to five points per m<sup>2</sup>). Our  
672 data set might therefore not serve well for capturing some ecological relevant variation in terrain and vegetation structures at  
673 scales below the 10 m x 10 m grain size. We believe that our data set is nonetheless valuable in providing ecologically relevant  
674 information at the geographical extent of Denmark.

675 While some of the descriptors in the presented data set such as elevation, slope and vegetation height are quite straightforward  
676 to interpret, the ecological meaning of other descriptors – for example those related to vegetation structure – may not be as  
677 obvious as they are influenced by multiple ecological and sensing methodology related factors. The *amplitude*, *point count*  
678 and *point proportion* descriptors are amongst those measures. For example, while the (non-calibrated) amplitude in the  
679 DHM/Point-cloud source data may generally relate to the reflectance properties of the surface that generated the return, the  
680 incident light angle, scattering and subsequent generation of echoes may result in several different surfaces generating similar  
681 amplitude signatures. Furthermore, the point counts may be influenced by a whole suite of factors, including incident light  
682 angle, scattering, density of flight strips covering a given cell, as well as canopy properties - most importantly the penetration  
683 ability. While standardising the point counts as proportions to the total counts may help to account for some of these factors,  
684 it is likely that notable uncertainties will remain even in the proportions especially for lower layers of the canopy. Nonetheless,  
685 we believe that these measures can be informative if appropriate care is taken in their interpretation.

686 Two code developments could enhance the EcoDes-DK15 processing workflow in efficiency and transferability: using gdal  
687 Python bindings and switching to an open-source point cloud handler. First, for practical reasons we reverted to using gdal  
688 binaries rather than the Python bindings as we encountered issues with the gdal bindings provided by the OPALS shell on our  
689 computational server. Solving this issue and using the bindings instead of the binaries could reduce hard drive access time and  
690 overheads from launching subprocesses and therefore potentially speed up the raster manipulations in the workflow. However,  
691 as the point cloud processing takes the majority of time (we estimate 75-80%) we did not invest further resources to do so in  
692 the first development round. Secondly, while our Python source code is open source and freely available, OPALS itself requires

693 the purchase of a software license, limiting the transferability of our code to projects which can afford the license. We did not  
694 explore alternatives to OPALS, but a redeveloped processing pipeline could make use of purely open source software  
695 benefiting from ongoing developments in the field, see for example the “Laserchicken” Python module (Meijer et al., 2020)  
696 and “lidR” R package (Roussel et al., 2020).

697

698 We believe that to realise the full potential of ALS derived data such as EcoDes-DK15 these data sets are ideally combined  
699 with other data sources including climate, field data and remote sensing observations. Climate data is especially relevant for  
700 addressing research on species-habitat relationships, distribution models and biodiversity studies and many studies have  
701 demonstrated the power of ALS observations in complementing climate data for such exercises (Coops et al., 2016; Zellweger  
702 et al., 2016). Like for other remote sensing products, field data is essential for validating inferences and putting biological  
703 meaning into ALS data (Coops et al., 2021) - this applies especially to the more complex structural vegetation measures in  
704 EcoDes-DK15. This could be achieved through field surveys combined with terrestrial and drone based ALS data, where the  
705 point density is much higher (e.g., Madsen et al., 2020). The potential benefits from fusing ALS data with other remote sensing  
706 products have been realised early on (Hyde et al., 2005) and demonstrated again since then (e.g., Coops et al., 2021;  
707 Montgomery et al., 2019; Manzanera et al., 2016). However, note that data fusion does not provide additional value in every  
708 use case (Xu et al., 2018; Ceballos et al., 2015; Boelman et al., 2016). We still believe that there is tremendous potential in  
709 combining EcoDes-DK15 with other types of remote sensing data. Fine-grain optical imagery could provide proxies for  
710 horizontal vegetation structure in grasslands where the vegetation is too small to be captured by the DHM/Point-cloud density  
711 (e.g., Malmstrom et al., 2017; Pazúr et al., 2021) and satellite derived time-series can provide unique temporal perspectives  
712 that describe parameters of seasonality (e.g., Boelman et al., 2016) and the historical context on disturbances and landcover  
713 change not captured in the single time-point ALS data (e.g., Senf et al., 2017; Pekel et al., 2016).

## 714 **6. Data availability**

715 The data is openly available under a Creative Commons by Attribution 4.0 license on Zenodo:

716 <https://doi.org/10.5281/zenodo.4756556> (Assmann et al., 2021)

717

718 A small example subset “teaser” (5 MB) covering the 9 km x 9 km of the Husby Klit area (Fig. 7) is available on the GitHub  
719 code repository:

720 [https://github.com/jakobjassmann/ecodes-dk-lidar/blob/master/manuscript/figure\\_6/EcoDes-DK15\\_teaser.zip](https://github.com/jakobjassmann/ecodes-dk-lidar/blob/master/manuscript/figure_6/EcoDes-DK15_teaser.zip)

721



722 **7. Code availability**

723 The source code for the processing pipeline is openly available under a simplified BSD license via GitHub:

724 <https://github.com/jakobjassmann/ecodes-dk-lidar>

725 **8. Conclusions**

726 Open data sets like EcoDes-DK15 will allow ecologists with limited computational resources and little expertise in handling  
727 LiDAR point clouds to use large-scale ALS data for their research. We see our efforts not only as a first step for providing  
728 ready-to-use descriptors of local vegetation and terrain features, but also for providing an example workflow and tools that  
729 allow for the replication of the processing. We have described and documented the measures of terrain and vegetation structure  
730 contained in the data set and pointed out possible applications and limitations. We are confident that EcoDes-DK15 provides  
731 a meaningful collection of ecological descriptors at a 10 x 10 m resolution for the extent of a whole country and we encourage  
732 the community to use our workflow and collection of codes as inspiration to process other large-scale ALS data sets in a similar  
733 manner. Ultimately, we hope the publication of this data set will help facilitate the uptake of ALS-derived information by  
734 ecological researchers and practitioners in Denmark and beyond.

735 **9. Author contributions**

736 All co-authors developed the data set with focus on its ecological relevance, providing input on the ecological meaning, spatial  
737 scale and calculation of the descriptors. JJA developed the code with input from JEM. JJA carried out the computations. JJA  
738 led the writing of the manuscript, with all co-authors contributing to the manuscript in a collaborative manner. SN provided  
739 funding and supervision for this project.

740 **10. Competing interests**

741 The authors declare that they have no conflict of interest.

742 **11. Acknowledgements**

743 We would like to thank Andr as Zlinszky for his contributions to earlier versions of the data set, Charles Davison for feedback  
744 regarding data use and handling, as well as Matthew Barbee and Zs ofia Koma for sharing their insights on the source data  
745 merger and Zs ofia's script to generate summary statistics for the different versions of the DHM point clouds. Funding for this  
746 work was provided by the Carlsberg Foundation (Distinguished Associate Professor Fellowships) and Aarhus University

747 Research Foundation (AUFF-E-2015-FLS-8-73) to Signe Normand (SN). This work is a contribution to SustainScapes –  
748 Center for Sustainable Landscapes under Global Change (grant NNF200C0059595 to SN).

## 749 12. References

- 750 Ackermann, F.: Airborne laser scanning—present status and future expectations, *ISPRS J PHOTOGRAMM*, 54, 64–67,  
751 [https://doi.org/10.1016/S0924-2716\(99\)00009-X](https://doi.org/10.1016/S0924-2716(99)00009-X), 1999.
- 752 ASPRS: LAS Specification Version 1.3 - R11, American Society for Photogrammetry & Remote Sensing, Bethesda, Maryland,  
753 2011.
- 754 ASPRS: LAS Specification 1.4 - R14, American Society for Photogrammetry and Remote Sensing, Bethesda, Maryland, 2019.
- 755 Assmann, J. J., Moeslund, J. E., Treier, U. A., and Normand, S.: EcoDes-DK15: High-resolution ecological descriptors of  
756 vegetation and terrain derived from Denmark’s national airborne laser scanning data set, Zenodo [data set],  
757 <https://doi.org/10.5281/zenodo.4756556>, 2021.
- 758 Bakx, T. R. M., Koma, Z., Seijmonsbergen, A. C., and Kissling, W. D.: Use and categorization of Light Detection and Ranging  
759 vegetation metrics in avian diversity and species distribution research, *Divers Distrib*, 25, 1045–1059,  
760 <https://doi.org/10.1111/ddi.12915>, 2019.
- 761 Beven, K. J. and Kirkby, M. J.: A physically based, variable contributing area model of basin hydrology / Un modèle à base  
762 physique de zone d’appel variable de l’hydrologie du bassin versant, *Hyrdol Sci B*, 24, 43–69,  
763 <https://doi.org/10.1080/02626667909491834>, 1979.
- 764 Boelman, N. T., Holbrook, J. D., Greaves, H. E., Krause, J. S., Chmura, H. E., Magney, T. S., Perez, J. H., Eitel, J. U. H.,  
765 Gough, L., Vierling, K. T., Wingfield, J. C., and Vierling, L. A.: Airborne laser scanning and spectral remote sensing give a  
766 bird’s eye perspective on arctic tundra breeding habitat at multiple spatial scales, *Remote Sens Environ*, 184, 337–349,  
767 <https://doi.org/10.1016/j.rse.2016.07.012>, 2016.
- 768 Böhner, J. and Selige, T.: Spatial Prediction Of Soil Attributes Using Terrain Analysis And Climate Regionalisation, *Göttinger*  
769 *Geographische Abhandlungen*, 115, 13–120, 2006.
- 770 Ceballos, A., Hernández, J., Corvalán, P., and Galleguillos, M.: Comparison of Airborne LiDAR and Satellite Hyperspectral  
771 Remote Sensing to Estimate Vascular Plant Richness in Deciduous Mediterranean Forests of Central Chile, *Remote Sens-*  
772 *Basel*, 7, 2692–2714, <https://doi.org/10.3390/rs70302692>, 2015.
- 773 Conrad, O., Bechtel, B., Bock, M., Dietrich, H., Fischer, E., Gerlitz, L., Wehberg, J., Wichmann, V., and Böhner, J.: System  
774 for Automated Geoscientific Analyses (SAGA) v. 2.1.4, *Geosci Model Dev*, 8, 1991–2007, [https://doi.org/10.5194/gmd-8-](https://doi.org/10.5194/gmd-8-1991-2015)  
775 [1991-2015](https://doi.org/10.5194/gmd-8-1991-2015), 2015.
- 776 Coops, N. C., Tompaski, P., Nijland, W., Rickbeil, G. J. M., Nielsen, S. E., Bater, C. W., and Stadt, J. J.: A forest structure  
777 habitat index based on airborne laser scanning data, *Ecol Indic*, 67, 346–357, <https://doi.org/10.1016/j.ecolind.2016.02.057>,  
778 2016.

779 Coops, N. C., Tompalski, P., Goodbody, T. R. H., Queinnec, M., Luther, J. E., Bolton, D. K., White, J. C., Wulder, M. A., van  
780 Lier, O. R., and Hermosilla, T.: Modelling lidar-derived estimates of forest attributes over space and time: A review of  
781 approaches and future trends, *Remote Sens Environ*, 260, 112477, <https://doi.org/10.1016/j.rse.2021.112477>, 2021.

782 Flatman, A., Rosenkranz, B., Evers, K., Bartels, P., Kokkendorff, S., Knudsen, T., and Nielsen, T.: Quality assessment report  
783 to the Danish Elevation Model (DK-DEM), Agency for Data Supply and Efficiency, Copenhagen, Denmark, 2016.

784 Freeman, T. G.: Calculating catchment area with divergent flow based on a regular grid, *Comput Geosci*, 17, 413–422,  
785 [https://doi.org/10.1016/0098-3004\(91\)90048-I](https://doi.org/10.1016/0098-3004(91)90048-I), 1991.

786 Froidevaux, J. S. P., Zellweger, F., Bollmann, K., Jones, G., and Obrist, M. K.: From field surveys to LiDAR: Shining a light  
787 on how bats respond to forest structure, *Remote Sens Environ*, 175, 242–250, <https://doi.org/10.1016/j.rse.2015.12.038>, 2016.

788 GDAL/OGR contributors: GDAL/OGR Geospatial Data Abstraction software Library, Open Source Geospatial Foundation,  
789 2018.

790 GDAL/OGR contributors: GDAL/OGR Geospatial Data Abstraction software Library, Open Source Geospatial Foundation,  
791 2021.

792 Geodatastyrelsen: Dataspecifikation for Danmarks Højdemodel Punktsky. Data version 2.0 - Januar 2015., Geodatastyrelsen,  
793 Copenhagen, 2015.

794 Grohmann, C. H.: Effects of spatial resolution on slope and aspect derivation for regional-scale analysis, *Computers &*  
795 *Geosciences*, 77, 111–117, <https://doi.org/10.1016/j.cageo.2015.02.003>, 2015.

796 Gruber, S. and Peckahm, S.: Land-Surface Parameters and Objects in Hydrology, in: *Geomorphometry: Concepts, Software,*  
797 *Applications*, vol. 33, edited by: Hengl, T. and Reuter, H. I., Elsevier, 293–308, 2008.

798 Guo, X., Coops, N. C., Tompalski, P., Nielsen, S. E., Bater, C. W., and John Stadt, J.: Regional mapping of vegetation structure  
799 for biodiversity monitoring using airborne lidar data, *Ecol Inform*, 38, 50–61, <https://doi.org/10.1016/j.ecoinf.2017.01.005>,  
800 2017.

801 Haralick, R. M.: Ridges and valleys on digital images, *Comput Vision Graph*, 22, 28–38, <https://doi.org/10.1016/0734->  
802 [189X\(83\)90094-4](https://doi.org/10.1016/0734-189X(83)90094-4), 1983.

803 Horn, B. K. P.: Hill shading and the reflectance map, *P IEEE*, 69, 14–47, <https://doi.org/10.1109/PROC.1981.11918>, 1981.

804 Hyde, P., Dubayah, R., Peterson, B., Blair, J. B., Hofton, M., Hunsaker, C., Knox, R., and Walker, W.: Mapping forest structure  
805 for wildlife habitat analysis using waveform lidar: Validation of montane ecosystems, *Remote Sens Environ*, 96, 427–437,  
806 <https://doi.org/10.1016/j.rse.2005.03.005>, 2005.

807 IPBES: Global assessment report on biodiversity and ecosystem services of the Intergovernmental Science-Policy Platform on  
808 Biodiversity and Ecosystem Services., edited by: Brondizio, E. S., Díaz, S., and Settele, J., IPBES secretariat, Bonn, Germany.,  
809 2019.

810 Kopecký, M., Macek, M., and Wild, J.: Topographic Wetness Index calculation guidelines based on measured soil moisture  
811 and plant species composition, *Sci Total Environ*, 143785, <https://doi.org/10.1016/j.scitotenv.2020.143785>, 2020.

812 Leiterer, R., Furrer, R., Schaepman, M. E., and Morsdorf, F.: Forest canopy-structure characterization: A data-driven approach,  
813 *Forest Ecology and Management*, 358, 48–61, <https://doi.org/10.1016/j.foreco.2015.09.003>, 2015.

814 Leutner, B. F., Reineking, B., Müller, J., Bachmann, M., Beierkuhnlein, C., Dech, S., and Wegmann, M.: Modelling Forest  $\alpha$ -  
815 Diversity and Floristic Composition — On the Added Value of LiDAR plus Hyperspectral Remote Sensing, *Remote Sens*-  
816 *Basel*, 4, 2818–2845, <https://doi.org/10.3390/rs4092818>, 2012.

817 Levin, G.: Basemap03. Technical documentation of the method for elaboration of a land-use and land-cover map for Denmark,  
818 Aarhus University, DCE – Danish Centre for Environment and Energy, Aarhus, Denmark, 2019.

819 Lin, Y., Vosselman, G., Cao, Y., and Yang, M. Y.: Active and incremental learning for semantic ALS point cloud  
820 segmentation, *ISPRS J PHOTOGRAMM*, 169, 73–92, <https://doi.org/10.1016/j.isprsjprs.2020.09.003>, 2020.

821 Lopatin, J., Dolos, K., Hernández, H. J., Galleguillos, M., and Fassnacht, F. E.: Comparing Generalized Linear Models and  
822 random forest to model vascular plant species richness using LiDAR data in a natural forest in central Chile, *Remote Sens*  
823 *Environ*, 173, 200–210, <https://doi.org/10.1016/j.rse.2015.11.029>, 2016.

824 Madsen, B., Treier, U. A., Zlinszky, A., Lucieer, A., and Normand, S.: Detecting shrub encroachment in seminatural grasslands  
825 using UAS LiDAR, *Ecol Evol*, 10, 4876–4902, <https://doi.org/10.1002/ece3.6240>, 2020.

826 Malmstrom, C. M., Butterfield, H. S., Planck, L., Long, C. W., and Eviner, V. T.: Novel fine-scale aerial mapping approach  
827 quantifies grassland weed cover dynamics and response to management, *PLOS ONE*, 12, e0181665,  
828 <https://doi.org/10.1371/journal.pone.0181665>, 2017.

829 Manzanera, J. A., García-Abril, A., Pascual, C., Tejera, R., Martín-Fernández, S., Tokola, T., and Valbuena, R.: Fusion of  
830 airborne LiDAR and multispectral sensors reveals synergic capabilities in forest structure characterization, *GISci Remote Sens*,  
831 53, 723–738, <https://doi.org/10.1080/15481603.2016.1231605>, 2016.

832 Mao, L., Dennett, J., Bater, C. W., Tompalski, P., Coops, N. C., Farr, D., Kohler, M., White, B., Stadt, J. J., and Nielsen, S.  
833 E.: Using airborne laser scanning to predict plant species richness and assess conservation threats in the oil sands region of  
834 Alberta’s boreal forest, *Forest Ecol Manag*, 409, 29–37, <https://doi.org/10.1016/j.foreco.2017.11.017>, 2018.

835 McCune, B. and Keon, D.: Equations for potential annual direct incident radiation and heat load, *J Veg Sci*, 13, 603–606,  
836 <https://doi.org/10.1111/j.1654-1103.2002.tb02087.x>, 2002.

837 Meijer, C., Grootes, M. W., Koma, Z., Dzigan, Y., Gonçalves, R., Andela, B., van den Oord, G., Ranguelova, E., Renaud, N.,  
838 and Kissling, W. D.: Laserchicken—A tool for distributed feature calculation from massive LiDAR point cloud datasets,  
839 *SoftwareX*, 12, 100626, <https://doi.org/10.1016/j.softx.2020.100626>, 2020.

840 Moeslund, J. E., Arge, L., Bøcher, P. K., Dalgaard, T., Odgaard, M. V., Nygaard, B., and Svenning, J.-C.: Topographically  
841 controlled soil moisture is the primary driver of local vegetation patterns across a lowland region, *Ecosphere*, 4, art91,  
842 <https://doi.org/10.1890/ES13-00134.1>, 2013.

843 Moeslund, J. E., Zlinszky, A., Ejrnæs, R., Brunbjerg, A. K., Bøcher, P. K., Svenning, J.-C., and Normand, S.: Light detection  
844 and ranging explains diversity of plants, fungi, lichens, and bryophytes across multiple habitats and large geographic extent,  
845 *Ecol Appl*, 29, e01907, <https://doi.org/10.1002/eap.1907>, 2019.

846 Montgomery, J., Brisco, B., Chasmer, L., Devito, K., Cobbaert, D., and Hopkinson, C.: SAR and Lidar Temporal Data Fusion  
847 Approaches to Boreal Wetland Ecosystem Monitoring, *Remote Sens-Basel*, 11, 161, <https://doi.org/10.3390/rs11020161>,  
848 2019.

849 Moore, I. D., Grayson, R. B., and Ladson, A. R.: Digital terrain modelling: A review of hydrological, geomorphological, and  
850 biological applications, *Hydrol Process*, 5, 3–30, <https://doi.org/10.1002/hyp.3360050103>, 1991.

851 Morgan-Wall, T.: rayshader: Create Maps and Visualize Data in 2D and 3D, 2020.

852 Moudrý, V., Lecours, V., Malavasi, M., Misiuk, B., Gábor, L., Gdulová, K., Šímová, P., and Wild, J.: Potential pitfalls in  
853 rescaling digital terrain model-derived attributes for ecological studies, *Ecological Informatics*, 54, 100987,  
854 <https://doi.org/10.1016/j.ecoinf.2019.100987>, 2019.

855 Moudrý, V., Klápště, P., Fogl, M., Gdulová, K., Barták, V., and Urban, R.: Assessment of LiDAR ground filtering algorithms  
856 for determining ground surface of non-natural terrain overgrown with forest and steppe vegetation, *MEASUREMENT*, 150,  
857 107047, <https://doi.org/10.1016/j.measurement.2019.107047>, 2020.

858 Nord-Larsen, T., Riis-Nielsen, T., and Ottosen, M. B.: Forest resource map of Denmark: Mapping of Danish forest resource  
859 using ALS from 2014-2015, Department of Geosciences and Natural Resource Management, University of Copenhagen,  
860 Copenhagen, Denmark, 2017.

861 Pazúr, R., Huber, N., Weber, D., Ginzler, C., and Price, B.: A national extent map of cropland and grassland for Switzerland  
862 based on Sentinel-2 data, *Earth Syst Sci Data*, 1–14, <https://doi.org/10.5194/essd-2021-60>, 2021.

863 Pekel, J.-F., Cottam, A., Gorelick, N., and Belward, A. S.: High-resolution mapping of global surface water and its long-term  
864 changes, 540, 418–422, <https://doi.org/10.1038/nature20584>, 2016.

865 Peura, M., Silveyra Gonzalez, R., Müller, J., Heurich, M., Vierling, L. A., Mönkkönen, M., and Bässler, C.: Mapping a ‘cryptic  
866 kingdom’: Performance of lidar derived environmental variables in modelling the occurrence of forest fungi, *Remote Sens  
867 Environ*, 186, 428–438, <https://doi.org/10.1016/j.rse.2016.09.003>, 2016.

868 Pfeifer, N., Mandlbürger, G., Otepka, J., and Karel, W.: OPALS – A framework for Airborne Laser Scanning data analysis,  
869 *Comput Environ Urban*, 45, 125–136, <https://doi.org/10.1016/j.compenvurbsys.2013.11.002>, 2014.

870 Quinn, P., Beven, K., Chevallier, P., and Planchon, O.: The prediction of hillslope flow paths for distributed hydrological  
871 modelling using digital terrain models, *Hydrol Process*, 5, 59–79, <https://doi.org/10.1002/hyp.3360050106>, 1991.

872 Reback, J., McKinney, W., Bossche, J. V. den, jbrockmendel, Augspurger, T., Cloud, P., gfyong, Sinhrks, Klein, A., Tratner,  
873 J., She, C., Roeschke, M., Petersen, T., Ayd, W., Hayden, A., Hawkins, S., Schendel, J., Garcia, M., Jancauskas, V., Battiston,  
874 P., Seabold, S., chris-b1, h-vetinari, Hoyer, S., Overmeire, W., Mehayar, M., nouri, behzad, Kluyver, T., Whelan, C., and Chen,  
875 K. W.: pandas-dev/pandas: v0.24.2, Zenodo, <https://doi.org/10.5281/zenodo.3509135>, 2019.

876 Roussel, J.-R., Auty, D., Coops, N. C., Tompalski, P., Goodbody, T. R. H., Meador, A. S., Bourdon, J.-F., de Boissieu, F., and  
877 Achim, A.: lidR: An R package for analysis of Airborne Laser Scanning (ALS) data, *Remote Sens Environ*, 251, 112061,  
878 <https://doi.org/10.1016/j.rse.2020.112061>, 2020.

879 SAGA-GIS Tool Library Documentation v7.8.2: [http://www.saga-gis.org/saga\\_tool\\_doc/7.8.2/index.html](http://www.saga-gis.org/saga_tool_doc/7.8.2/index.html), last access: 28 June  
880 2021.

881 Senf, C., Pflugmacher, D., Hostert, P., and Seidl, R.: Using Landsat time series for characterizing forest disturbance dynamics  
882 in the coupled human and natural systems of Central Europe, *ISPRS J Photogramm*, 130, 453–463,  
883 <https://doi.org/10.1016/j.isprsjprs.2017.07.004>, 2017.

884 Sithole, G. and Vosselman, G.: Experimental comparison of filter algorithms for bare-Earth extraction from airborne laser  
885 scanning point clouds, *ISPRS J PHOTOGRAMM*, 59, 85–101, <https://doi.org/10.1016/j.isprsjprs.2004.05.004>, 2004.

886 Thers, H., Brunbjerg, A. K., Læssøe, T., Ejrnæs, R., Bøcher, P. K., and Svenning, J.-C.: Lidar-derived variables as a proxy for  
887 fungal species richness and composition in temperate Northern Europe, *Remote Sens Environ*, 200, 102–113,  
888 <https://doi.org/10.1016/j.rse.2017.08.011>, 2017.

889 Tweedy, P. J., Moriarty, K. M., Bailey, J. D., and Epps, C. W.: Using fine scale resolution vegetation data from LiDAR and  
890 ground-based sampling to predict Pacific marten resting habitat at multiple spatial scales, *Forest Ecol Manag*, 452, 117556,  
891 <https://doi.org/10.1016/j.foreco.2019.117556>, 2019.

892 Valbuena, R., O'Connor, B., Zellweger, F., Simonson, W., Vihervaara, P., Maltamo, M., Silva, C. A., Almeida, D. R. A.,  
893 Danks, F., Morsdorf, F., Chirici, G., Lucas, R., Coomes, D. A., and Coops, N. C.: Standardizing Ecosystem Morphological  
894 Traits from 3D Information Sources, *Trends Ecol Evol*, S0169534720300811, <https://doi.org/10.1016/j.tree.2020.03.006>,  
895 2020.

896 Van Rossum, G. and Drake Jr, F. L.: Python reference manual, Centrum voor Wiskunde en Informatica Amsterdam, 1995.

897 Vierling, K. T., Vierling, L. A., Gould, W. A., Martinuzzi, S., and Clawges, R. M.: Lidar: shedding new light on habitat  
898 characterization and modeling, *Front Ecol Environ*, 6, 90–98, <https://doi.org/10.1890/070001>, 2008.

899 Vo, A.-V., Laefer, D. F., and Bertolotto, M.: Airborne laser scanning data storage and indexing: state-of-the-art review, *Int J*  
900 *Remote Sens*, 37, 6187–6204, <https://doi.org/10.1080/01431161.2016.1256511>, 2016.

901 Wagner, W., Ullrich, A., Ducic, V., Melzer, T., and Studnicka, N.: Gaussian decomposition and calibration of a novel small-  
902 footprint full-waveform digitising airborne laser scanner, *ISPRS J Photogramm*, 60, 100–112,  
903 <https://doi.org/10.1016/j.isprsjprs.2005.12.001>, 2006.

904 Wang, L. and Liu, H.: An efficient method for identifying and filling surface depressions in digital elevation models for  
905 hydrologic analysis and modelling, *Int J Geogr Inf Sci*, 20, 193–213, <https://doi.org/10.1080/13658810500433453>, 2006.

906 Weiss, A.: Topographic position and landforms analysis, in: Poster presentation, ESRI user conference, San Diego, CA, 2001.

907 Xu, C., Manley, B., and Morgenroth, J.: Evaluation of modelling approaches in predicting forest volume and stand age for  
908 small-scale plantation forests in New Zealand with RapidEye and LiDAR, *Int J Appl Earth Obs*, 73, 386–396,  
909 <https://doi.org/10.1016/j.jag.2018.06.021>, 2018.

910 Yokoyama, R.: Visualizing Topography by Openness: A New Application of Image Processing to Digital Elevation Models,  
911 *Photogramm Eng Rem S*, 68, 257–265, 2002.

912 Zellweger, F., Baltensweiler, A., Ginzler, C., Roth, T., Braunisch, V., Bugmann, H., and Bollmann, K.: Environmental  
913 predictors of species richness in forest landscapes: abiotic factors versus vegetation structure, *J Biogeogr*, 43, 1080–1090,  
914 <https://doi.org/10.1111/jbi.12696>, 2016.  
915